RHEINISCH-
WESTFÄLISCHE
TECHNISCHE
HOCHSCHULE
AACHEN

Chair of Flight Dynamics
Prof. Dr.-Ing. W. Alles

Study Thesis

Numeric Simulation of a Glider Winch Launch

cand. ing. Christoph G. Santel

2008

Advising Tutor: Dipl.-Ing. Jan Nowack

Task

The question of the optimized winch launch arises from the current advancements in glider performance and increase in glider mass. As a first step in modeling the winch launch, a winch, cable and pilot model was introduced into an existing six-degree-of-freedom glider simulation in MATLAB/Simulink already developed at the Chair of Flight Dynamics.

This model is to be enhanced. More comprehensive winch and pilot models shall be configured on the basis of enhanced data that is now available. When possible, the cable should be modeled in FEM. Subsequently, the parameters of the simulation are to be varied in order to gain insight into the optimized winch launch.

The following steps are to be completed in the frame of this thesis:

- Research of existing research papers and data on the topic
- Enhancement of the simulation (winch, cable, pilot behavior)
- Variation of simulation parameters (cable properties, weak links, pilot behavior, wind)
- Analysis of the results as they pertain to an optimal winch launch
- Comprehensive documentation of all work done

Contents

List of Figures

List of Symbols

Notation	
A	Cross Section
C	Coefficient
E	Energy, Modulus of Elasticity
F	Force
G, H	Transfer Functions
I	Moment of Inertia
K	Control Constant
L	Unstrained Cable Segment Length
M	Mach Number, Moment, Molecular Mass
N	Rotational Speed
P	Power
R	Universal Gas Constant, Location
Re	Reynolds Number
S	Safety Margin
T	Time, Temperature, Cable Tension, Torque
V	Velocity
X, Y, Z	Cartesian Forces
c	Strain-Speed-Proportional Stress Coefficient
d	Diameter, Distance
e	Unit Vector
f	Power Lever Setting, Frequency
g	Gravitational Acceleration
h	Unit Step Response, Altitude
i	Gear Transmission Ratio
j	Identification Number of Cable Element or Mass Point
k	Scaling Factor
l	Strained Cable Segment Length
m	Mass
n	Number of Cable Elements or Mass Points, Load Factor
p	Air Pressure
r	Relative Location
s	Complex Variable of the Laplace Domain
t	Time
p, q, r	Cartesian Rotational Speeds
u, v, w	Cartesian Velocities
x, y, z	Cartesian Coordinates

continued on next page

Δ	Difference
Φ	Bank Angle
Θ	Pitch Angle
Ψ	Heading
α	Angle of Attack
χ	Glider-Winch-Angle
ε	Strain
γ	Angle of Climb
η	Elevator Deflection, Degree of Efficiency
λ	Angle between Glider's Longitudinal Axis and Cable Force
μ	Viscosity Coefficient
ρ	Density
ω	Angular Frequency

Indices

0	Initial Value at Beginning of Simulation, Sea-Level Condition
AC	Aircraft
C	Cable
D	Cable Drum, Aerodynamic Drag
CS	Camshaft
DL	Driveline
E	Winch Engine, External
G	Glider
N	Integrating Time Constant
NE	Never Exceed
O	Winch Operator
P	Pilot
S	Stall
T	Target
V	Derivative Time Constant
W	Winch
a	Aerodynamic Coordinates
d	Delay Time
f	Aircraft-fixed Coordinates
g	Geodetic Coordinates
hf	Higher Frequency
i	Neuromuscular Derivative Time
k	Track-fixed coordinates
lf	Lower Frequency

Abbreviations

6DoF	Six Degrees of Freedom
CG	Center of Gravity
Datcom	Data Compendium
FEM	Finite Element Method
IAS	Indicated Airspeed
ICAO	International Civil Aviation Organisation
ISA	International Standard Atmosphere
GUI	Graphical User Interface

Conventions in Mathematical Notation

Z	Scalar Term, Scalar Value of $\vec{Z}$
$\|Z\|$	2-Norm of Z
$\vec{Z}$	Vector
$\underline{Z}$	Second Order Tensor
$\dot{Z}$	Derivative of Z in Direction of Time
Z'	Amplitude
$Z :=$	Definition of Z

Typeset Conventions

Italicize	Name of File and Path from Simulation's Main Directory
Small Caps	Action to be taken by the simulation user
`Typewriter`	Name of Simulink Block

0.1 Foreword

This study thesis has been written at the Chair of Flight Dynamics at the RWTH Aachen University as part of a more comprehensive research project pertaining to the behavior of gliders in flight which has been funded by the German Federal Ministry of Transport, Building and Urban Affairs.

The primary goal of this thesis is to provide a quantitative analysis of the mechanic loads occurring during the winch launch of a glider and to supply numeric data for future optimization of the winch launch process. This has been attempted to achieve by developing a computer simulation in the environment of MATLAB/Simulink.

While the first half of the written report is intended as documentation of the development process and as a reference manual, the second half uses the presented simulation as a tool for grading and discussing the winch launch. By varying different parameters, the influences of these variations are identified and an attempt is made to compare these results to practical experiences.

A project of the magnitude of this simulation is achieved through the helpful input of many different people and institutions. At this point I would like to thank everyone who has been involved in this project. Specifically, I would like to mention and thank Dipl.-Ing. Jan Nowack for his tuition of my study thesis and for him providing the academic guidance needed in the sometimes frustrating, yet often rewarding process of writing this thesis. Dipl.-Ing. Andreas Gäb was also very helpful and always eager to answer my numerous questions about working with MATLAB/Simulink. For many evenings of creative discussion and the opportunity to "kick ideas back and forth", I also need to thank cand. phys. Jens Richter. The different proof-readers who aided in bringing this thesis into a presentable form are not to be forgotten and deserve their share of praise. Special thanks in this regard go to Kathrin Herkenrath. At last, a sincere thank you also is extended to the companies Tost Startwinden GmbH and Rosenberger Tauwerk GmbH for providing information on their products.

Aachen, Germany,
in the fall of 2008

Christoph Santel

1 Background

©JM-Fotoservice

Figure 1.1: Rear View Study of an ASK 21 Glider during Winch Launch

1.1 Introduction

In most parts of western Europe and many other parts of the world, the winch launch is the preferred method of launching gliders. Its relatively low operating costs, feasible operator requirements and relatively low complexity have ensured the widespread usage of winches in modern day soaring and provide many glider sites with a reliable and inexpensive method of launch. A basic impression of the winch launch can be gained from the side and rear view studies given in figures 1.1 and 1.2. In comparison to the aerotow launch, where the whole propulsion equipment is airborne and must be designed for acceptable flight performance and maintained according to governing aeronautical regulations, the winch is completely ground based. This makes the use of lightweight design techniques in the construction of a glider winch not compulsory and also alleviates the regular maintenance requirements while using simpler technologies. Also, the operator does not need to be a fully rated pilot for piston-engine airplanes.

While the major advancements in glider design - such as the use of composite materials and laminar airfoils - have been driven by competitive considerations, the

design of winches lacks such a driving force. With the widespread introduction of composite high performance gliders and the ensuing increase in maximum takeoff weight, it has become necessary to equip winches with stronger engines, though the basic technology has changed little since the widespread introduction of winches in the 1950's and 1960's. Yet, the most recent innovation in this field has been the replacement of the steel cables used to tow the gliders by synthetic cables. Completely new drivetrain designs, being powered by electric motors, have been in operation for several years, though most of them are prototypes or proof-of-concept designs.

Generally, the technical research in winch launching has been very low-key, providing only little written analysis on the nature of the winch launch. Additionally, it should be mentioned that the few documents which regulate the construction and operation of glider winches, such as the "Operational Requirements for Glider and Motorglider Winches" (Tec86) of the German Aeroclub, mostly rely on values of experience and rough estimates in their assessment of the acting loads.

Even though a previous thesis with similar content has already been treated at the Chair of Flight Dynamics by Kloss (Klo07), the goal of this thesis and simulation is to provide a means of comparison and quantification of aspects pertaining to the winch launch process.

Figure 1.2: Side View Study of an ASK 21 Glider during Winch Launch

1.2 The Winch Launch

The winch launch is a highly dynamic method of launching gliders to a sufficiently safe altitude for free flight. Derek Piggott describes the concept in a simple manner: "The basic principle of winch [...] launching is the same as launching a kite. The aircraft is pulled along the ground until it has sufficient speed to lift off" (Pig96). After lifting off, the glider will then - after having reached a sufficiently safe altitude - transition to a climb which is characterized by steep pitch and climb angles. As the horizontal distance between the glider and winch decreases, the climb and pitch angles slowly decrease until the cable is either manually or automatically released when the aircraft is in the vicinity of the winch. At this point, the glider should be in nearly steady and horizontal flight.

Apel (Ape96) defines six distinct phases of the winch launch which are illustrated in figure 1.3. Specifically, these phases are:

1. before ground roll
2. ground roll and lift off
3. transition to climb
4. climb
5. transition to level flight and cable release
6. after cable release

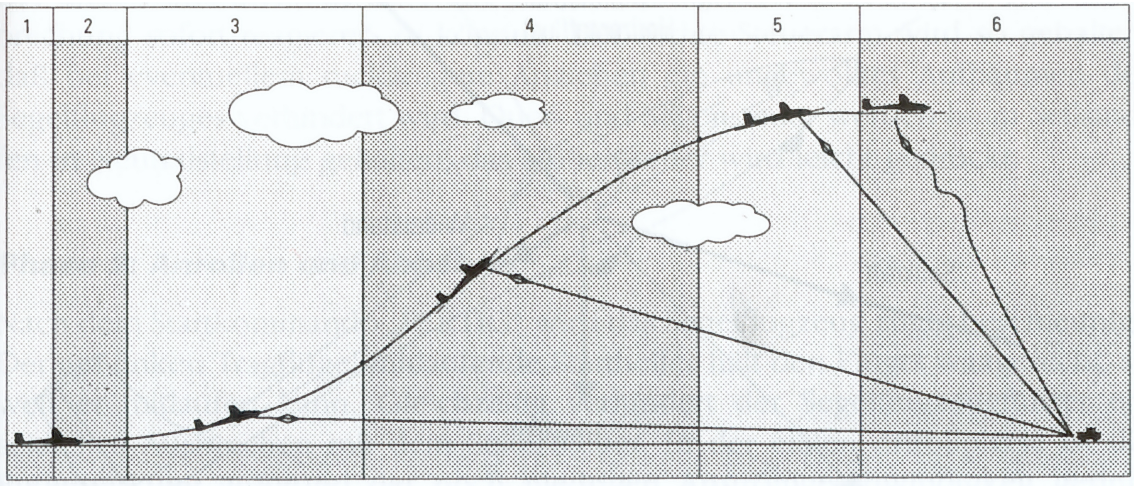

from (Ape96)

Figure 1.3: Phases of Winch Launching

The most critical phase is considered to be the transition to the climb, since the aircraft will have a relatively high pitch angle at relatively low altitude. In the event of a cable break, the airspeed will usually decay swiftly. To prevent a stall at low altitude the nose will need to be quickly lowered in order to prevent the airspeed from falling below the stall speed.

For reasons discussed later, only phases 3 through 5 are accurately depicted in the developed simulation. The simulation terminates at the moment of cable release, and does not regard free flight[1].

1.3 Necessary Equipment

The cable is connected to the glider through a hook. During aerotow the tow cable is usually attached as far forward of the aircraft's center of gravity (CG) as possible. This increases static lateral and longitudinal stability and relieves pilot workload. However, high longitudinal stability is uncalled-for during the winch launch. It would prevent the high pitch and climb angles used to gain altitude quickly and mounting the tow hook close to the CG becomes necessary. Most modern gliders are equipped with both, a nose hook for aerotows as well as a CG hook for ground launches.

Additionally, several safety components are required by the German "Glider Operation Regulations" (Seg03). They are depicted in figure 1.4 and need to be mounted in the following order at the end of the cable closest to the glider:

- standardized tow ring
- leading cable, enshrouded in a stiff hose to prevent loops from forming
- weak link, according to aircraft flight manual
- intermediate cable
- drag chute
- clipper hook, for quick disconnection of auxiliary cable equipment
- main cable

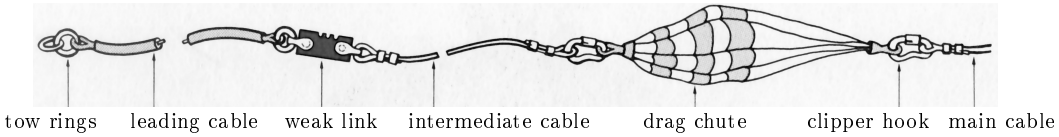

from (Mai93)

Figure 1.4: Necessary Auxiliary Equipment for Winch Tow Cable

1.4 Development Considerations

The numeric nature of this thesis makes it necessary to analyze a specific winch and glider combination. This contrasts the highly generic value of an analytical analysis which is often independent of specific equipment. To provide significant results, the analyzed aircraft and winch need to be sufficiently generic in their nature. Therefore,

[1] phase 6 of the winch launch

the ASK 21 primary training glider, developed by Alexander Schleicher GmbH & Co. Segelflugzeugbau of Poppenhausen, Germany, was chosen as the simulated glider. The ASK 21 is a composite two-seat training glider in widespread use worldwide and its aerodynamics and flight performance are similar to other aircraft of the composite primary training fleet. For the purpose of this simulation, the ASK 21 is said to be representative of this fleet. Also, the availability of a flight mechanics model, drawn from previous research of the ASK 21 at the Chair of Flight Dynamics, was a factor in selecting this glider type.

While data for a specific aircraft - the ASK 21 - was readily available, few specifics on certain winch models were at hand. Through the generous assistance of Tost Startwinden GmbH of Assling, Germany, it was possible to obtain technical data on one of the company's winch types. Yet many parameters still had to be estimated. Though Tost is one of the market leaders in the construction of glider winches, many winches in operation in Germany and worldwide are self-constructed single-unit productions. This causes the general validity of the winch model to be lower than the glider model.

The cable and glider are both moving through space during the simulated winch launch, whereas the winch is considered to remain stationary. Hence, the cable and gliders are both modeled with six degrees of freedom (6DoF) in cartesian space using the principles of Newtonian mechanics. But the full expressiveness of the 6DoF could not be exhausted. Time restrictions to this thesis allowed only for an implementation of a basic pilot model and control law that controls only the aircraft's longitudinal motion. This causes all following simulations to be of a symmetric nature and the following analysis of the winch launch to be valid on the presumption of quasi-two-dimensionality. In the future, the inclusion of control laws to influence the aircraft's lateral movement is possible and would utilize the possibilities of the 6DoF simulation more comprehensively. The author would welcome any such additions in the future.

1.5 Simulation Environment in MATLAB/Simulink

The portrayed models have been implemented using the R2007b version of MATLAB, created and distributed by the The MathWorks Inc. of Natick, Massachusetts, USA. This is an object-oriented programming language and development environment with focus on vectorial and matrix calculations. One of MATLAB's tools is Simulink. It allows for the graphical definition of mathematical models analogous to block diagrams. The individual elements of such models, called blocks, interact through signals with each other. Capabilities such as the ability to define transfer functions in the Laplace complex variable domain and the possibility of using embedded MATLAB code make Simulink a fitting tool for control engineering modeling and numeric flight simulation.

For the standard calculations of flight simulation, the Chair of Flight Dynamics has developed a library of commonly used MATLAB/Simulink blocks. Tasks executed by this library might include coordinate transformations, calculation of aircraft inertia, determination of international standard atmosphere values and so forth. This MATLAB/Simulink library proves an adequate basis for this study thesis.

2 Models and Simulation

For the purpose of this simulation the problem of the glider winch launch has been broken down into three interfaced primary components - winch, cable and glider - which interact through their outputs with each other. In order to depict the influence of human operators on the winch and aircraft and to achieve closed loop control over these primary components, rudimentary pilot and winch operator models are integrated as feedback loops. This interaction of the five independent models is depicted in block diagram 2.1. Methods regarding standard atmospheric influence are integrated into the relevant models, making the International Standard Atmosphere (ISA) the sixth used in this simulation. The different natures of the physical phenomena within each model make the use of different coordinate systems reasonable. A description of each of the used systems is given in appendix A. Appendix B provides a user's guide for easier handling of the simulation by the end user.

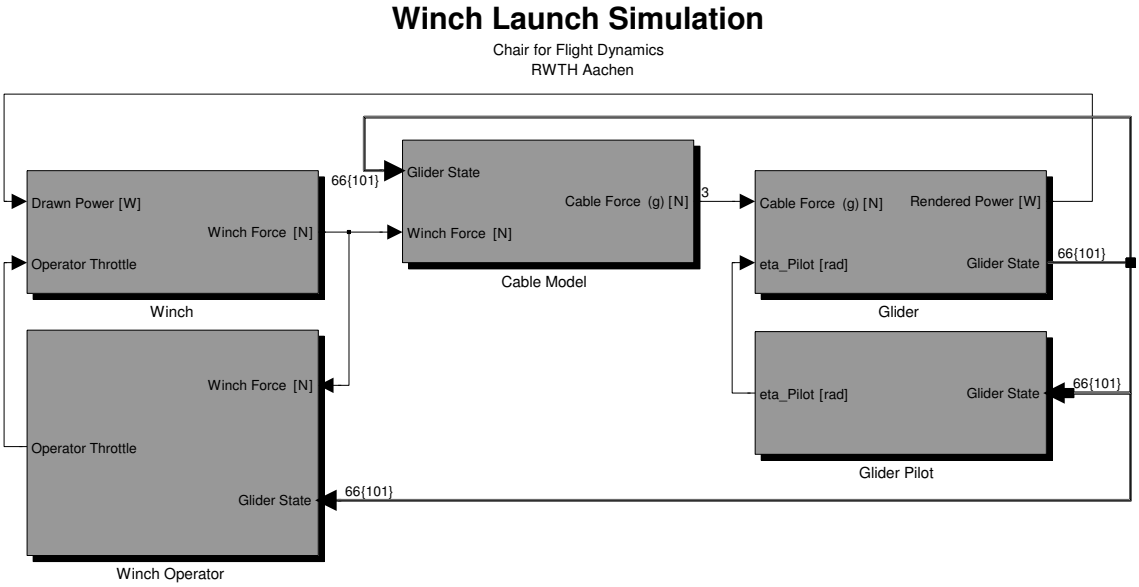

Figure 2.1: Block Diagram of Simulation

From a developmental standpoint, this simulation is the enhancement of a generic six degrees of freedom (6DoF) flight simulation in MATLAB/Simulink which has been previously developed at the Chair of Flight Dynamics (Gäb07). Several blocks regarding the peculiarities of the winch launch were added to the existing aircraft model, which was then integrated into the rest of the simulation. This facilitated the use of an existing graphical user interface previously intended for the generic aircraft simulation.

2.1 Implemented MATLAB/Simulink Blocks

2.1.1 Aircraft Model

The used generic MATLAB/Simulink aircraft model, which for the purpose of this simulation has been integrated into the `Glider` block, is further divided into several blocks; one each for calculation of acting forces and moments, the 6DoF equations of motion, terminating conditions, events, calculation of wind, and blocks for modifying the glider's state data bus with wind information and adding current ISA values to the bus. The aerodynamic and inertial data of the Schleicher ASK 21, which has been drawn from previous research projects at the Chair of Flight Dynamics, is stored in the files *ask21aero_edited.mat* and *ask21_moi.mat* respectively.

Through the use of nonlinear coefficients the aerodynamic moments and forces acting on the aircraft are calculated. The used model is limited in that it only regards an obstruction-free quasi-static airstream around the aircraft. This causes the aircraft's behavior during the phases of flight in which it is exposed to strong ground effect - namely the take-off[1] run in this simulation - not to be depicted accurately. As soon as the virtual glider reaches its initial climb attitude and an altitude of approximately one wingspan above ground level, the aerodynamic results are said to be within acceptable accuracy.

The aerodynamic forces and moments, along with the forces and moments induced into the glider by the winch cable are then passed to the aircraft's rigid body inertial model. This, again, is in accordance with the conventional approaches of basic flight dynamics in which the aircraft is defined as a point mass. Its translational inertia is regarded by the aircraft mass m_{AC} and its rotational inertia is depicted in an inertial tensor $\underline{I}_{\mathrm{AC}}$. These parameters are interfaced with the glider's state through the Newtonian basic equations of motion, as can be drawn from Alles (All05) or Brockhaus (Bro01).

One of the shortcomings of the rigid body model is that it does not regard aeroelastic effects. Especially when high load factors are present - as is the fact during the main climb phase - the validity of this assumption has to be challenged. The bending of the wing is influenced by the wing's geometric moment of inertia, the wingspan and load factor. This results in large displacement of the wing's centerline, especially in open class gliders. But the deformations in primary training gliders are usually smaller and not considered for our purposes.

A further assumption is that the quasi-static, undisturbed airflow around the aircraft is said to be incompressible. All occurring airspeeds in the simulation are expected to be smaller than the ASK 21's $V_{NE} = 280km/h$ IAS (Ale80), being equivalent under standard conditions to $M_{NE} = 0.23$. As is general practice for $M < M_{NE} < 0.3$, the compressibility effects are considered to be of small magnitude and negligible.

Aircraft Model Modifications

The generic aircraft model - which is taken from previous work at the Chair of Flight Dynamics - needs to be modified to regard the specifics of the winch launch. Block

[1] phase 2 of the winch launch

diagram 2.2 illustrates this. The original aircraft model has not been designed to regard acting external forces, except aerodynamic lift and drag, thrust and gravity. Yet, the force being exerted by the tow cable onto the glider is the primary means of increasing the glider's sum of potential and kinetic energy. It is self-evident that an interface for the cable-induced loads has to be introduced. This `Cable Load Interface` is located in the `Glider` model's `External Forces and Moments` block.

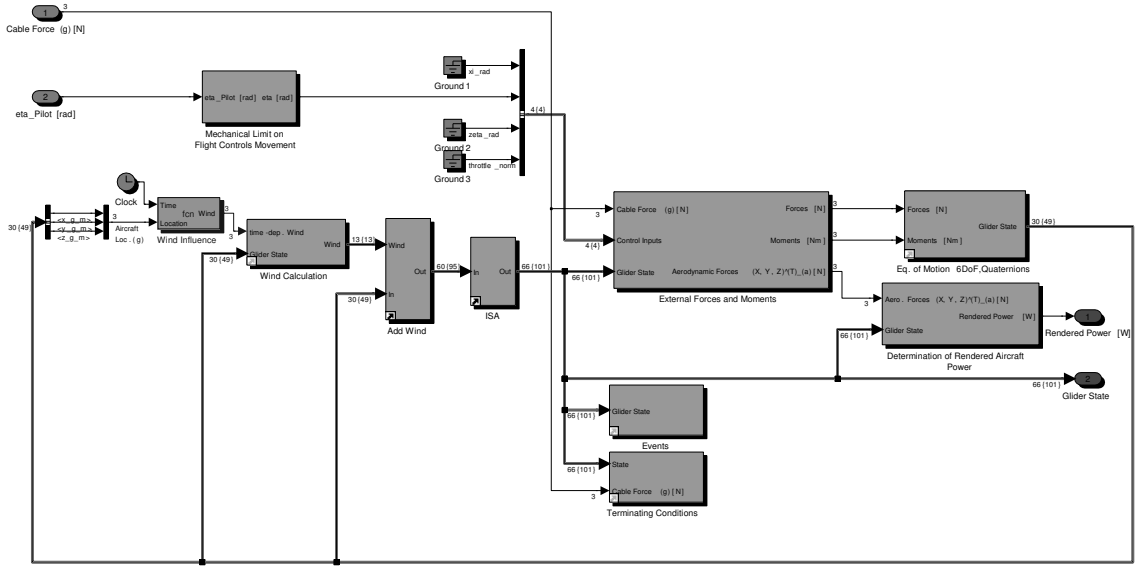

Figure 2.2: Block Diagram of the Glider Model

The force $\vec{F}_{G,C}$ induced from the cable into the glider is passed into the interface, which then calculates the resulting moment $\vec{M}_{G,C}$ of $\vec{F}_{G,C}$ force around the glider's center of gravity. With $\vec{R}_{\text{CG-Hook}}$ being the location vector of the glider's CG tow hook, $\vec{M}_{G,C}$ follows to

$$\vec{M}_{G,C} = \vec{R}_{\text{CG-Hook}} \times \vec{F}_{G,C} \tag{2.1}$$

$\vec{F}_{G,C}$ and $\vec{M}_{G,C}$ are then added to the aerodynamic and gravitational loads of the generic model and the respective sums are passed into the inertial calculations.

As the input loads into the generic model's inertial calculations are formulated in aircraft-fixed coordinates, and as $\vec{F}_{C,G}$ is given by the `Cable` block in geodetic coordinates, a coordinate transformation becomes necessary. $\vec{R}_{\text{CG-Hook}}$ is also most easily formulated in aircraft-fixed coordinates.

To properly declare the termination of the simulation at the moment of cable release [2], an additional terminating method `Cable Release Mechanism` has to be devised and integrated into the glider's `Terminating Conditions` block. The ASK 21 uses a standard CG tow hook supplied by Tost GmbH Fluggerätebau of Munich, Germany. This hook releases the cable automatically when the force $\vec{F}_{G,C}$ exceeds a critical angle λ_{Release} to the $\vec{x}_f$-axis in the aircraft's plane of symmetry. With $F_{G,C,x}$ and $F_{G,C,z}$ being the $\vec{x}_f$- and $\vec{z}_f$-components of $\vec{F}_{G,C}$, the cable angle λ follows to

$$\lambda = sin^{-1} \frac{F_{G,C,z}}{\sqrt{F_{G,C,x}^2 + F_{G,C,z}^2}} \tag{2.2}$$

[2] transition from phase 5 to phase 6 of winch launch according to Apel (Ape96)

The method terminates the simulation as soon $\lambda > \lambda_{\text{Release}}$ and ensures that no termination occurs if no cable-induced force is present.

Due to the elastic nature of the cable model used, cable vibration might occur. In the case that the winch-induced tension has not yet properly engaged[3] at the glider end of the tow cable, forces of extremely small magnitude[4] with $\lambda > \lambda_{\text{Release}}$ might exist. To prevent a termination of the simulation, all $\vec{F}_{G,C}$ with $F_{G,C} < F_{G,C,min}$ are treated as if no cable induced force were present at the release mechanism[5].

The pilot-commanded elevator deflection η_P might differ from the actual elevator deflection η due to restricted movement of the flight controls. This is described in the block `Mechanical Limit on Flight Controls Movement` by linking the signal η_P with η through a saturation block to ensure that $\eta \in [\eta_{min}, \eta_{max}]$.

The block `Calculation of Rendered Aircraft Power` determines the currently rendered power P_{AC} by the aircraft. Power is rendered by the aircraft's movement through the geopotential field (subscript $_{pot}$), its changes in its kinetic state (subscript $_{kin}$) as well as through aerodynamic drag (subscript $_{D}$):

$$P_{\text{AC}} = P_{\text{pot}} + P_{\text{D}} + P_{\text{kin}} \tag{2.3}$$

with

$$P_{\text{pot}} = -m_{\text{AC}} \cdot \vec{g} \cdot \vec{v}_{\text{AC}} \tag{2.4}$$

$$P_{\text{D}} = -\vec{v}_{\text{AC}} \cdot \vec{F}_D \tag{2.5}$$

$$P_{\text{kin}} = \frac{d}{dt}\left(\frac{1}{2} m_{\text{AC}} \cdot \vec{v}_{AC} \cdot \vec{v}_{\text{AC}} + \frac{1}{2}\vec{\omega}_{\text{AC}} \cdot (\underline{I}_{\text{AC}}\vec{\omega}_{\text{AC}})\right) \tag{2.6}$$

$$\tag{2.7}$$

and

$$\vec{\omega}_{\text{AC}} := \begin{pmatrix} p \\ q \\ r \end{pmatrix}_{\text{AC}} \tag{2.8}$$

To clarify the sign convention, it should be stated that an increase in an energetic state of the glider carries with it $P > 0$.

In order to exploit the specific advantages of each coordinate system, different systems are used to calculate the different power components. P_{pot} is determined in geodetic ($_g$), P_{D} in aerodynamic ($_a$) and P_{kin} in aircraft-fixed ($_f$) coordinates. The rendered aircraft power P_{AC} will later be parsed into the `winch` block for further calculations.

Wind acting on the glider in flight is easily determined using the `Wind Influence` block. It utilizes a vectorial method allocated in the file *WindVectorField.m*, allowing for the definition of wind vector fields varying in time and location.

As previously mentioned in section 1.4 and described in more detail in section 2.1.4, only longitudinal motion of the glider is controlled by the pilot model. This forces a disregard of the yawing and pitching moments produced by mounting the

[3] For further discussion of numeric engagement of the cable solution, refer to section 2.3.

[4] in the order of $10^{-9}N$

[5] This could be physically interpreted as friction keeping the ring engaged in the tow hook when only minor a tow force $\vec{F}_{G,C}$ acts on the glider.

CG tow hook out of the aircraft's plane of symmetry. To achieve this properly in the later studied cases, the $\vec{y}_{\text{CG-Hook},f}$-component of CG hook's location vector must be set to $\vec{y}_{\text{CG-Hook},f} = 0$.

2.1.2 Winch Model

Though having been treated theoretically by Riddell (Rid98), the modeling of inertial effects on the winch during the launch could not be found in previous numeric simulations. For example, the works of the Akaflieg Karlsruhe (HS98) as well previous research at the Chair of Flight Dynamics by Kloss (Klo07) have modeled the winch solely as a source of a time-variant torque and force acting upon the tow cable. With the creation of this winch model, an attempt has been made to provide a generic, yet significant physical model. It allows for signal feedback routings pertaining to the influence of the cable and glider upon the winch as well as the addition of a winch controller model.

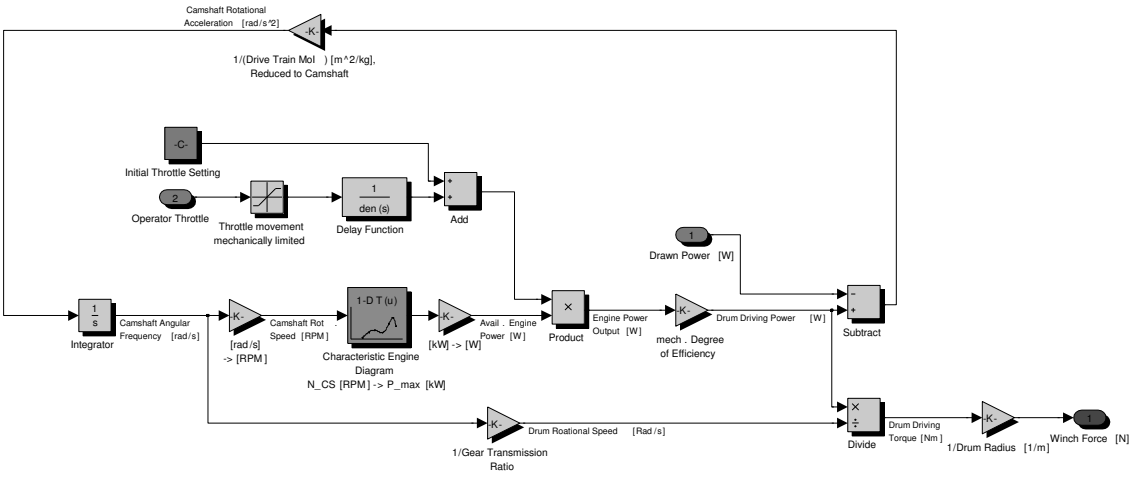

Figure 2.3: Block Diagram of the Winch

Using the methods of automotive engineering as presented by Kiencke and Nielsen (KN00), the winch is represented by a driveline and engine model. The winch model's block diagram is given in figure 2.3. As previously discussed, the design of winches often varies. The most prominent variations are in the used engine - being either operated on gasoline or diesel fuel - as well as the use of a torque converter, or lack thereof, in the driveline. Due to the availability of data, it was decided to represent a driveline without torque converter being powered by a supercharged diesel engine. The driveline itself is said to consist only of the following rotating elements: the camshaft, an ideal gearbox, one cable drum and a shaft connecting the cable drum to the gearbox. These components are said to be stiff to torque. Mechanical losses of all elements are regarded in one driveline degree of efficiency η_{DL} while the inertial behavior is regarded in one scalar driveline moment of inertia reduced onto the engine camshaft $I_{\text{DL, red}}$. Though intended as a model of a two drum winch, the second cable drum is not regarded since in normal operation only one drum is engaged to the drivetrain using a clutch.

The centerpiece of the winch simulation is the engine's characteristic diagram providing a correspondence between the engine crankshaft's revolving speed N_{CS}

and the maximum power output $P_{\mathrm{E,\,max}}(N_{\mathrm{CS}})$. This diagram, given in figure 2.4, has been implemented into a lookup table using cubic spline interpolation between nodes to provide a continuously differentiable power output over time. For operations outside the data interval provided, cubic spline extrapolation is used. A result of this extrapolation is that the engine output power rapidly declines when the engine is being operated above the camshaft revolving speed for maximum power The same is true for moving operations into relatively low crankshaft speeds. These effects coincide with actual observations of internal combustion engines.

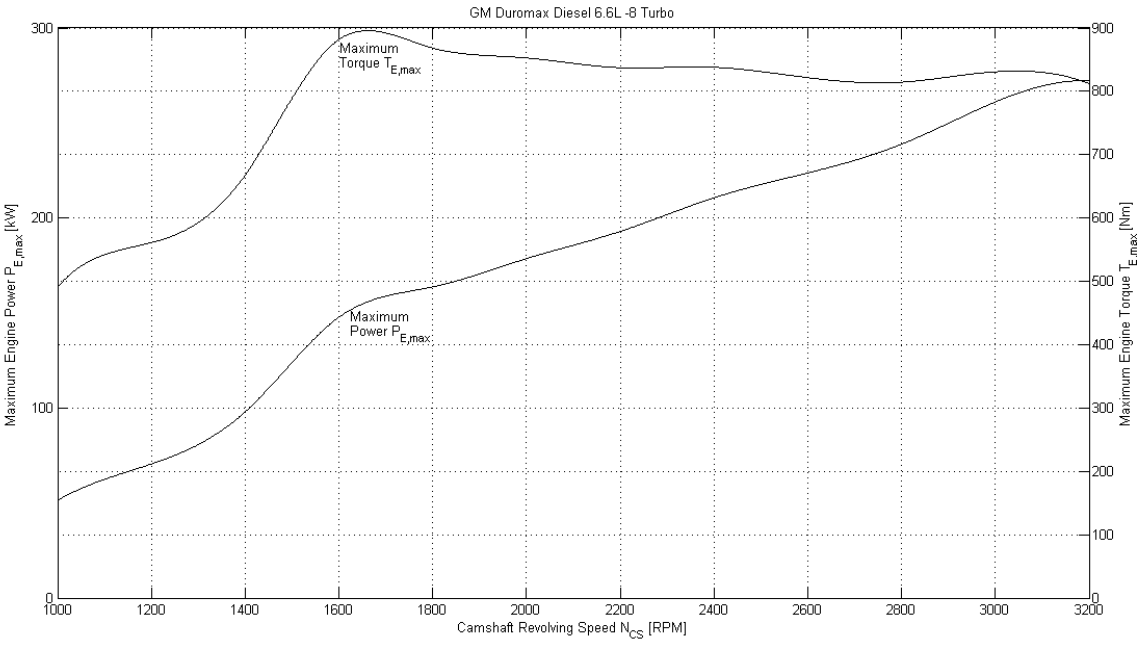

Data Source: (Gen08)

Figure 2.4: Characteristic Power Curve

Tost Startwinden GmbH kindly provided information on its Series 010 winches as well as the GM V8 454 gasoline engine used in this product. Unfortunately, during the development of the winch model, this engine proved to be inadequate. It lacks the torque necessary for the analysis of higher winch forces in section 3.2.6 and made the implementation of a higher torque diesel engine necessary. The GM Duromax Diesel 6.6L turbocharged diesel engine was chosen, which is used in the Skylaunch 3 winch (Sky08) produced by Skylaunch Ltd of Shropshire, Great Britain. Though data on the basic engine performance was obtained though General Motors (Gen08) no quantitative correlation between engine throttle setting and the engine's actual power output was given. Therefore, the throttle influence f has been approximated to be a linear scaling factor of the maximum power output, reducing it to the actual engine power output. To account for the slight delay in availability of engine power following a change in the throttle setting, the linear scaling factor is adjusted through a first order delay element with a relatively short derivative time. The actual throttle setting is determined by filtering the operator commanded throttle setting through a saturation block so that $f \in [f_{\min}, f_{\max}] = [f_{\min}, 1]$. The upper limit of the block is set to allow full throttle operation and the lower limit is selected to approximate idle operation.

The engine output power, adjusted for mechanical losses along the driveline through a constant degree of efficiency η_{DL}, as well as the camshaft rotational speed ω_{CS}, the gear transmission ratio i and drum diameters d_d are then used to determine the scalar force $F_{C,W}$ exerted by the winch onto the cable. Also, power difference between the engine output power and the power drawn by other simulation components $P_E - P_{\mathrm{Drawn}}$ is said to accelerate the driveline's revolving speed, causing a feedback loop within the winch driveline.

The data provided by Tost Startwinden was limited to the cable drum diameter and gear transmission ratio of its Series 010 winches and little other quantitative information on winch properties was found. This made it necessary to estimate many properties, such as mechanical degrees of efficiency, moments of inertia of the driveline, or influence of the butterfly valve setting on the engine. A more general winch model, lacking the specifics of a certain winch type, is the result of these approximations and use of values of experience. In comparison to the aircraft model, which is considered a precise enough representation of the Schleicher ASK 21, the winch model cannot be said to represent one specific type. It should much rather be interpreted as being similar to many of the winches with two cable drums in operation today.

2.1.3 Cable Model

A detailed description of the tow cable's deformation is necessary to accurately determine the cable tow force $\vec{F}_{G,C}$ acting on the glider. Due to the non-conservative nature of the aerodynamic forces acting on the cable, in addition to the conservative gravitational influence, it was decided to model the cable by the means of a dynamic *Finite Element Method* (*FEM*).

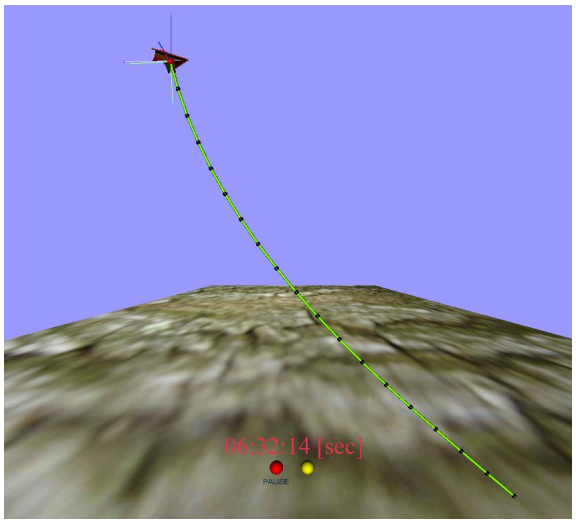

from (WLO07)

Figure 2.5: Computer-Rendering of the Cable Model in a Kite Simulation

The model - placed in the `Cable Model` block - is based upon the works of Williams, Lansdorp and Ockels (WLO07) and has been originally developed for the simulation of tethered kites in electric power generation through a laddermill.

Figure 2.5 shows a computer-rendering of the deformed cable in Williams', Lansdorp's and Ockels' kite simulation. Due to the high dynamic similarity between a tethered kite - which in a laddermill is reeled in and out at low frequency - and a glider being launched, this model is adequate. Though Williams, Lansdorp and Ockels (WLO07) present an inelastic model, provisions are already made to easily include elastic calculations. Due to this, the cable tension is modeled as being of damped linear elastic nature using a variation of Hooke's law together with a damping term. The block diagram of the cable model as it is implemented in this thesis is given in figure 2.6.

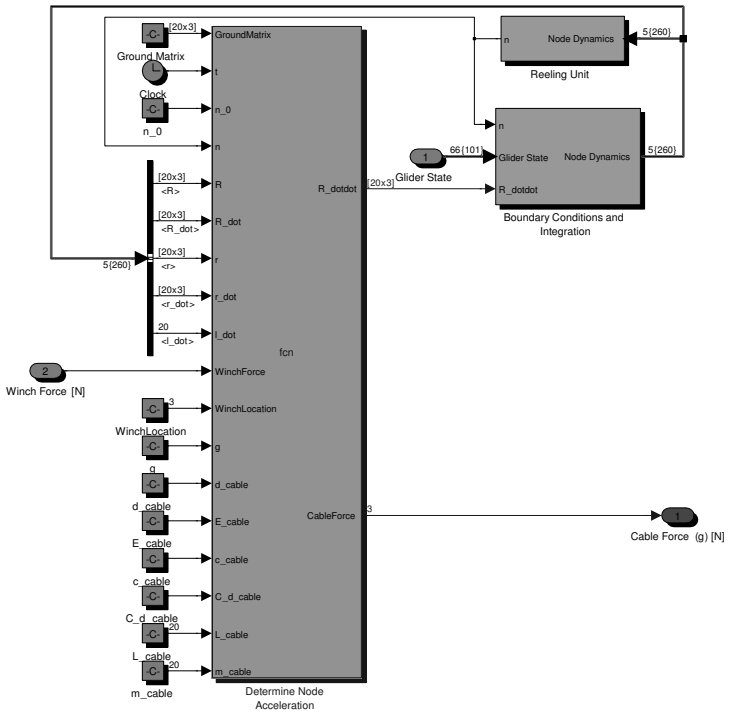

Figure 2.6: Block Diagram of the Cable Model

As a leading note: To facilitate references to Williams, Lansdorp and Ockels (WLO07) more easily, it has been decided to adopt the nomenclature and symbols used by them for the description of the cable model. It might differ slightly from the nomenclature of the remaining sections.

At the beginning of the simulation, the cable is discretized into n_0 discrete masses interconnected by massless elastic cylinders. Enumeration starts with the mass point closest to the glider and increases on its way to the winch. The iterative variable j is used to identify parameters pertaining to the jth lumped mass as well as to the cylinder between the j and $j+1$th masses.

The free cable length and the closely related free cable mass vary in time since the cable is reeled onto the winch drum during the launch. Whereas n is the current number of discrete mass points, the nth mass is removed when the segment length l_n between the last cable element and the winch falls below a predetermined length $l_{\min} = k^* \cdot l_{\text{ref}}$. In this case k^* is a scaling factor for an arbitrary reference length l_{ref}. This mathematical representation of reeling the cable onto the drum is represented in the `Reeling Unit` block.

The acceleration of each mass point is dependent upon the sum of internal and external forces acting on it. Because of this, the embedded MATLAB function block `Determine Node Acceleration` calculates the total acceleration acting on each cable mass point in geodetic coordinates by determining each of the acting internal and external forces at each mass point. These forces are then determined via methods stored in further *.m*-files.

External forces, namely aerodynamic drag and gravity, are modeled in direct accordance with Williams, Lansdorp and Ockels (WLO07). The presented algorithms for the calculation of each of the external forces have been placed in the *CableDrag.m* and *CableGravity.m* files respectively. For the specifics of the determination of the external forces, it is deemed appropriate to point the reader to (WLO07), as this section has been adopted precisely as described.

As mentioned before, the internal forces are determined through a damped linear elastic model, the respective method being accessible within the *CableTension.m* file. Dietz and Mupende (DM04) use a similar model when analyzing the interaction between synthetic cables and winch drums.

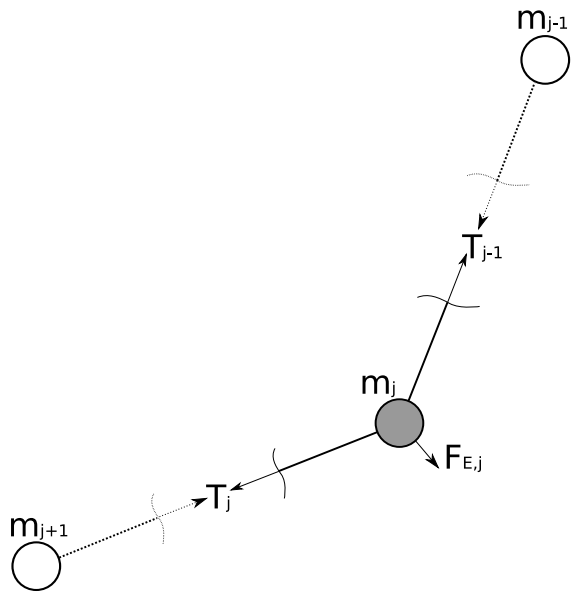

Figure 2.7: Illustration of Forces Acting on the jth Discrete Cable Mass

The magnitude of the tension T_j in the jth cable element is easily found by using a damped form of Hooke's law;

$$T_j = \underbrace{A_C \cdot E_C \cdot \varepsilon_j}_{\text{linear elastic term}} + \underbrace{A_C \cdot c_C \cdot \dot{\varepsilon}_j}_{\text{linear damping term}} = A_C \left(E_C \cdot \varepsilon_j + c_C \cdot \dot{\varepsilon}_j\right) \tag{2.9}$$

whereas A_C is the cable cross section and ε_j is the strain experienced by the jth element. E_c is the cable's modulus of elasticity and c_C is a strain-speed-proportional cable stress coefficient. The cable cross section is directly related to the cable diameter d_C by $A_C = \frac{\pi}{4} \cdot d_C^2$ while cross section contraction due to strain is neglected because of the braided nature of cables. By also relating the jth element strain ε_j to the respective strained and unstrained lengths l_j and L_j of the element, the tension

magnitude can be expressed as

$$T_j = \frac{\pi}{4} \cdot d_C^2 \cdot \left[E_C \cdot \left(\frac{l_j}{L_j} - 1 \right) + c_C \cdot \frac{\dot{l}_j}{L_j} \right] \tag{2.10}$$

As perfect flexibility is assumed in the cable, only axial tension forces can be transmitted, the tension force $\vec{T}_j$ acting in the jth segment is easily oriented by using the axial orientation of the jth cable element. The oriented tension force $\vec{T}_j$ is

$$\vec{T}_j = T_j \cdot \vec{e}_j = \frac{\pi}{4} \cdot d_C^2 \cdot \left[E_C \cdot \left(\frac{l_j}{L_j} - 1 \right) + c_C \cdot \frac{\dot{l}_j}{L_j} \right] \cdot \vec{e}_j \tag{2.11}$$

with the unit vector $\vec{e}_j$ describing the orientation of the j-th cable element.

$$\vec{e}_j = \frac{1}{l_j} \cdot \vec{r}_j = \frac{1}{l_j} \cdot \left(\vec{R}_j - \vec{R}_{j+1} \right) \tag{2.12}$$

Taking the results from the methods of the *CableDrag.m*, *CableGravity.m* and *CableTension.m* files, the ensuing cable dynamics are determined within the `Determine Node Acceleration` block as follows. The total force $\vec{F}_j$ acting on the jth mass point m_j is said to be

$$\vec{F}_j = \vec{F}_{E,j} + \vec{T}_{j-1} - \vec{T}_j \tag{2.13}$$

if $\vec{F}_{E,j}$ is the sum of all external forces acting upon the jth mass point. Therefore, the mass point acceleration $\ddot{\vec{R}}_j$ trivially follows as

$$\ddot{\vec{R}}_j = \frac{1}{m_j} \vec{F}_j \tag{2.14}$$

The temporal integrals $\dot{\vec{R}}_j$ and $\vec{R}_j$, of course, are the speed and location of the jth mass point. Equation 2.13 is also illustrated in figure 2.7.

To properly depict the glider launch within the cable model, several boundary conditions must be regarded:

1. The location of the first cable mass point at $j = 1$ is identical to the location of the glider's CG tow hook. This is of course also true for the relevant derivatives.

$$\vec{R}_1 = \vec{R}_{\text{CG-Hook}} \tag{2.15}$$
$$\dot{\vec{R}}_1 = \dot{\vec{R}}_{\text{CG-Hook}} \tag{2.16}$$
$$\ddot{\vec{R}}_1 = \ddot{\vec{R}}_{\text{CG-Hook}} \tag{2.17}$$
$$\tag{2.18}$$

2. Since the first mass point m_1 and the glider's CG tow hook are kinematically identical, the total force acting onto the first mass point is in fact the cable force acting onto the glider.

$$\vec{F}_{G,C} = \vec{F}_1 \tag{2.19}$$

3. The magnitude of the tension T_n acting onto the cable element closest to the winch ($j = n$) is defined by the magnitude of the force $F_{C,W}$ that is exerted by the winch onto the cable.

$$T_n = F_{C,W} \Rightarrow \vec{T}_n = F_{C,W} \cdot \vec{e}_n \tag{2.20}$$

As of now, the basic cable properties such as mean cable density ρ_C, cable diameter d_C, modulus of elasticity E_C and drag coefficient $C_{D,C}$ are kept constant across the length of the cable. In practice, this assumption is deeply violated by the placement of a drag chute and other auxiliary equipment between the actual tow cable and the glider CG hook. Due to the much higher drag per unit length acting on the drag chute - even in its collapsed form during the actual launch process - the glider end of the cable in practice is expected to deflect further against the direction of flight than the numeric results presented here. In the future, an incorporation of varying the above mentioned cable parameters over the cable length can be thought possible.

Another source of errors is the behavior of the cable model during the ground roll and initial climb phases of the winch launch[6]. The actual cable will be dragged over the surface of the airfield which is not implemented into the simulation. This causes the actual cable to experience a further friction force oriented against the direction of movement as long as is in contact with the ground and an additional force compensating the effects of gravity. Both of these forces are not regarded in the simulation and therefore limit its accuracy to the time after all of the cable is fully airborne[7].

Currently, the power rendered by the cable is also neglected. It is assumed that the kinetic and potential energies of the glider as well as the aerodynamic dissipation power of the glider are of much greater magnitude than those equivalent conservative and dissipating powers induced by the cable movement. The same is also assumed for the changes in internal elastic energy of the cable.

As a final note on cable models: Etkin (Etk98) has treated the motion of a cable in a similar manner as presented by Williams, Lansdorp and Ockels (WLO07). But he concentrates on the source and description of instabilities created by the cable motion.

For the numeric results, it was necessary to choose a particular cable for the reference simulation settings in section 3.1.1. A synthetic cable is chosen in the reference case, because lately these have often displaced the previously used steel cables on glider winches. Rosenberger Tauwerk GmbH of Lichtenberg, Germany, kindly provided data on its Liros-series of synthetic winch cables, which is implemented in the reference cable model.

2.1.4 Human Controller Models

Winch Operator Model

The purpose of the winch operator model is to stabilize the winch force $F_{C,W}$ exerted onto the tow cable around a given target force F_T. In order to achieve this goal, the winch operator has been modeled to act as a compensatory single-loop controller,

[6] phases 2 and 3
[7] This usually occurs in Apel's phase 3 of the winch launch (Ape96).

adjusting the winch's throttle in an attempt to stabilize the aforementioned force. It is presumed that operating the winch is a similar task to the longitudinal speed control of a motor vehicle. Kiencke and Nielsen state that in automotive control modeling, human driver behavior is often modelled as that of a PID controller (KN00).

These assumptions allow the winch operator to be modelled as a PID controller. The controller's transfer function follows to

$$G_{fF}(s) = \frac{f_O(s)}{F_{C,W}(s) - F_T(s)} = K_{fF} \cdot (1 + \frac{1}{T_{N,fF} \cdot s} + T_{V,fF} \cdot s) \tag{2.21}$$

with the input term being the difference between the winch force and target force $F_{C,W} - F_T$. As output term acts the winch operator commanded throttle setting f_O. The straightforward nature of the winch operator model becomes evident in its block diagram 2.8.

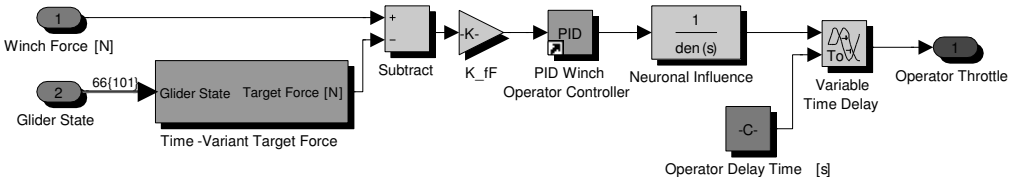

Figure 2.8: Block Diagram of the Winch Operator Model

Since excessive forces acting onto the glider at the beginning of the launch might bring the aircraft into a difficult to control state for the pilot, the winch operator will usually gradually increase winch power. Due to this, the target force is not a static parameter, but rather time-dependent. Through the use of ramp, saturation and first order delay elements, a function has been defined which increases the target force from an initial value $F_{T,0}$ in a continuously differentiable manner to a final target force $F_{T,\max}$. The slope of the used ramp-function defines the nominal rate of change of the target force $\frac{dF_T}{dT}$.

A winch operator will usually decrease the throttle setting as the glider approaches its cable release point to lower wear on material. To allow for this, the actual target force is determined by multiplying the previously described differentiable target force function with the cosine $\cos(\chi)$ of the glider-winch-angle. The glider-winch-angle χ is defined as being the angle between the location vector of the glider's initial location[8] $(-\vec{x}_W)$ as seen from the winch and the glider's current position $(\vec{x}_{\mathrm{AC}} - \vec{x}_W)$, also seen from the winch.

$$\chi := (-\vec{x}_W) \angle (\vec{x}_{\mathrm{AC}} - \vec{x}_W) \tag{2.22}$$

Using the law of cosines, χ follows to

$$\chi = \cos^{-1}\left(\frac{|-\vec{x}_W|^2 + |\vec{x}_{\mathrm{AC}} - \vec{x}_W|^2 - |\vec{x}_{\mathrm{AC}}|^2}{2 \cdot |-\vec{x}_W| \cdot |\vec{x}_{\mathrm{AC}} - \vec{x}_W|}\right) \tag{2.23}$$

For simplification, the calculation of χ and the differentiable target force function and its multiplication with $\cos(\chi)$ are all implemented within the `Time-Variant Target Force` block.

[8] This is the origin of the geodetic coordinate system.

It should be mentioned that modelling the winch operator as a force controller is only a rough first-order approximation. The force exerted onto the cable by the winch is usually not directly obvious to the winch operator. An actual operator will usually regard multiple other influences such as cable sag, engine noise and vibration, camshaft revolution speed and wind[9]. All of these influences, together with the operator's experience, will determine his or her actions on the throttle. It appears that winch operation could best be modeled through fuzzy logic, as is recommended by Henning and Kutscha (HK03). However, the winch operator model presented above will provide sufficiently smooth force transitions for the purpose of this simulation and is taken to be acceptable.

As a closing note on the subject of winch operators, several assistance systems need to be mentioned. At the Leverkusen airfield in Germany (ICAO-Code: EDKL), Dipl.-Ing. Markus Potthoff of the "Luftsportclub Bayer Leverkusen" has experimented with the club's winch by installing resistance straining gauges near the drums. With these, he was able to determine the winch's deformation near the drum suspension and experimentally determine the reaction force exerted by the cable onto the winch. These measurements were then provided to the operator in visual and audible form via electronics. This system allows for the feedback of the winch force to the operator and closes the control loop in a similar manner to the above mentioned winch operator model. Yet, the system has not gone past the experimental stadium.

The Wilhelm Nosbüsch GmbH of Haan/Rheinland, Germany, offers a telemetry system as an alternative operator assistance setup (Wil07). It informs the winch operator of the glider's airspeed by measuring the dynamic pressure electronically and transmitting it to a winch-side receiver. The data is then processed and passed to a display, being easily accessible to the operator. Though offered commercially, this system is not in widespread use either.

Pilot Model

As previously mentioned, the time constraints to this thesis allowed only for a simple pilot model controlling the longitudinal motion. Through several superpositioned control laws an elevator deflection η_P is commanded. This control structure becomes obvious in the pilot model's block diagram 2.9. Yet, all other pilot inputs into existing flight controls, such as ailerons, speed brakes, or rudder, are not considered.

Quite similar to the winch operator model, the pilot model's goal is to stabilize the glider around a target dynamic pressure[10] $p_{\mathrm{dyn},T}$. At the same time, the pilot serves in the role of a pitch damper to lessen or to suppress the glider's phugoid motion.

Dynamic pressure / airspeed control is achieved with the `IAS Controller` block, which in turn is being governed by the transfer function of a PID controller:

$$G_{\eta,p_{\mathrm{dyn}}}(s) = \frac{\eta_{\mathrm{IAS}}(s)}{p_{\mathrm{dyn}}(s) - p_{\mathrm{dyn},T}} = K_{\eta p_{\mathrm{dyn}}} \cdot (1 + \frac{1}{T_{N,\eta p_{\mathrm{dyn}}} \cdot s} + T_{V,\eta p_{\mathrm{dyn}}} \cdot s) \qquad (2.24)$$

[9] The wind, and especially its variations in intensity, is often challenging to gauge for the winch operator.

[10] Recall that for incompressible calculations the IAS is a representation of the dynamic pressure.

Here the target dynamic pressure $p_{\mathrm{dyn},T}$ is - in contrast to the target tow force $F_T(t)$ - independent of time.

Parallel to the `IAS Controller`, a simple pitch damper is placed for modifying the aircraft's dynamic behavior. This is realized with a simple proportional transfer function.

$$G_{\eta q}(s) = \frac{\eta_q(s)}{q_{\mathrm{AC}}(s)} = K_{\eta q} \tag{2.25}$$

A problem which arises with pure IAS control in the manner described is that the pilot would command the aircraft to climb at excessive angles of pitch at low altitude. Most flight training curricula strongly discourage such a maneuver, due to the insufficient recovery altitude available in the event of a cable break at low altitude. It is more typical for a pilot to leave the flight controls near a trimmed neutral position during initial climb and only to make minor adjustments in pitch and pitch speed. Only once a perceived safety altitude is reached, the pilot then transitions into controlling airspeed.

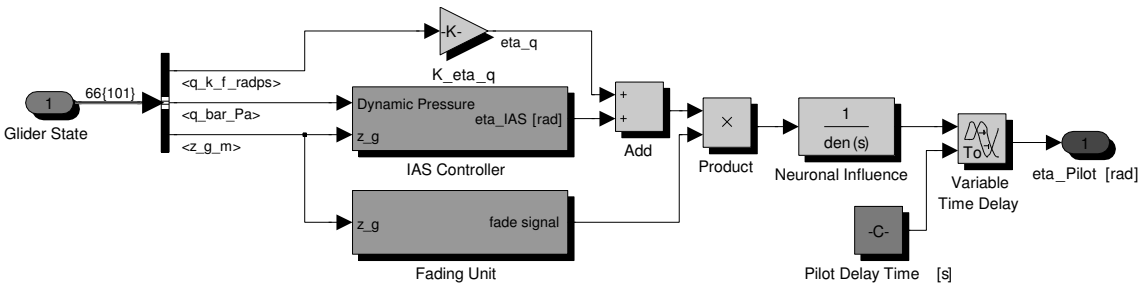

Figure 2.9: Block Diagram of the Pilot Model

To emulate this behavior, the sum of the `IAS controller` and pitch damper is multiplied with the output of a fading function. This `Fading Unit` block consists of a non-oscillating second-order delay element, experiencing a unit-step input in the moment the aircraft passes a predetermined safety altitude h_{Safety}. The unit step response of this second-order delay element

$$h_{\mathrm{Safety}}(t) = \begin{cases} 0 & t < t_{\mathrm{Safety}} \\ 1 - \frac{1}{T_1+T_2}(T_1 \cdot e^{\frac{t_{\mathrm{Safety}}-t}{T_1}} - T_2 \cdot e^{\frac{t_{\mathrm{Safety}}-t}{T_2}}) & t \geq t_{\mathrm{Safety}} \end{cases} \in [0,1) \tag{2.26}$$

is the output of the `Fading Unit` block. t_{Safety} is the moment at which the safety altitude is reached. T_1 and T_2 are characteristic times of the second order delay element.

The given signal routing makes certain that flight control inputs, except for a trim deflection η_{Trim}, are suppressed at low altitudes. Due to the location of the CG tow hook and the resulting moment $\vec{M}_{G,C}$ induced by the cable force $\vec{F}_{G,C}$, the aircraft will gently pitch up during the early climb phase. Additional airspeed control and pitch damping will be faded online only once a safety altitude is reached, steepening the climb angle.

Comments on Human Controller Models

Through his research in human-machine interfaces, Johannsen (Joh93) recommends augmenting human commanded actions with an additional transfer function to regard neuromuscular first order delays, psychological anticipation and delay times.

For this reason, the transfer function

$$H(s) = \frac{1}{1 + T_i \cdot s} \cdot e^{T_d \cdot s} \tag{2.27}$$

has been added to the winch operator as well as pilot models. The effects of this transfer function is minor in comparison to the transfer function of the PID controller representing the human decision process, though a slight effect on the stability of the controlled systems remains. Also, Alles (All80) regards the human influences in a similar manner.

Human controller models of the presented type are very rudimentary in comparison to the complexity of the human decision making process involved in controlling technical processes. The multitude of influences on human behavior is still often difficult to regard adequately for cybernetic consideration.

Especially in regard to the fact that the three-dimensional control of a glider in a winch launch - with all available flight control surfaces - is a high work load situation for the pilot which demands his or her utmost attention, the presented PID model is very basic.

The prognosis of the control parameters in human controller models, such as control factors, derivative and integrating times, is equally challenging. These parameters have been determined manually by operating each controller (winch operator and pilot) at first in an unstable, oscillating manner and then iteratively adjusting the parameters to stabilize the controller. This operation in the vicinity of the stability limit is assumed to regard the human decision process accurately enough.

2.1.5 Atmospheric Model / Wind Influence

In order to provide the calculated data in a compatible format with other aeronautical research, the atmospheric influence has been modeled in accordance with the ICAO's International Standard Atmosphere. At the beginning of the simulation, the aircraft is initialized at sea level, where standard atmospheric conditions prevail.

Even though the original generic aircraft model had interfaces for either time-dependent or location-dependent winds and gusts, these provisions were deactivated and ignored. This renders the original GUI inputs for wind non-operational and prevents accidental numeric "contamination" of the input data. In the current simulation, a time- and location-dependent three-dimensional wind vector field can be defined within the *WindVectorField.m*. The method stored in the file is then called at the appropriate times by the `Aircraft` and `Cable Model` blocks.

For the purpose of this simulation, the atmospheric movement is decoupled from the movement of the aircraft and cable through the air. This causes only the influence of the air onto the solid bodies to be considered, while the retroactions of the solid bodies onto the wind behavior are neglected.

For reasons of numeric effort within the `Cable Model`, it was decided not to calculate the air density through the `International Standard Atmosphere` block

in the Chair of Flight Dynamics library, but to perform these calculations in a small method stored in the *AirDensity.m* file. As can be easily derived from the thermodynamic ideal gas model of the ISA (Hen08), the air density within the troposphere is given as

$$\rho(h) = \frac{M_{\text{Air}}}{R} \cdot \frac{p_0}{T_0 + \frac{\partial T}{\partial h} \cdot h} \cdot \left(1 + \frac{\frac{\partial T}{\partial h} \cdot h}{T_0}\right)^{\frac{-g \cdot M_{\text{Air}}}{R \cdot \frac{\partial T}{\partial h}}} \tag{2.28}$$

Most glider flying takes place using convective thermal or orographic ridge lift within the troposphere. Only on rare occasions using wave lift do gliders pass the tropopause and climb to stratospheric altitudes. Since these specific operations are irrelevant for the launch simulation, the limitations by only regarding density distribution within the troposphere are of no significant effect.

Yet, as most glider flights are thermal flights and the favorable convective instabilities form predominantly during the warm summer month of the year, winches in operation are often exposed to "hot and high" conditions of high density altitude. A means for degrading winch performance for temperature- and elevation-induced effects on air density has not yet been included.

As already mentioned in sections 1.4, 2.1.1 and 2.1.4, no control mechanism to regulate lateral motion has been implemented in the simulation so far. This requires all sideways directed forces to be suppressed, so that the $v_{\text{Wind},f}$-component becomes $v_{\text{Wind},f} = 0$ in the ensuing analysis.

2.2 Provision of Data

The simulation's comprehensive model is stored in the *generic6DoF.mdl* file in the main directory. This is also the location of the aircraft's aerodynamic and inertial parameters, which are stored in the MATLAB files *ask21aero_edited.mat* and *ask21_moi.mat*. These are loaded with the generic simulation's GUI into the Simulink model. Also, several aircraft specific initial values of the simulation are stored under *Trimmpunkte/WinchLaunch.mat*. All other parameters specific to the winch simulation are stored under *WinchLaunchParameters.mat*, whereas this MATLAB variables file is created with the MATLAB script *WinchLaunchParameters.m*.

2.3 Engagement of Numeric Solution

The initial conditions of the glider and cable during the first iterative step are unaccelerated, steady movements with an strained cable. This is rooted in the fact that the incorporated 6DoF simulation initializes in unaccelerated and steady state of the aircraft. The cable is also initialized in a straight line between the glider's CG tow hook and the winch. One result of this is an initial iterative propagation of the additional strain, caused by gravity, along the cable. This takes several iteration steps to reach the glider and causes a slight oscillation of the cable force exerted onto the aircraft. The numeric solution will only stabilize after the simulation has run through several time steps. Since the beginning of the simulation - when the numeric solution has not yet engaged properly - is prone anyways to the previously

described physical errors, such as not regarded aircraft ground effect or cable friction on the airfield surface, this is readily accepted.

2.4 Further Limits of Models

Apart from the previously mentioned characteristics and limitations, several further points need to be mentioned. The aircraft model is that of a rigid body system, defined as a point mass. The glider's aerodynamic and flight mechanic behavior has been parameterized in flight tests conducted at the Chair of Flight Dynamics. The resulting linear coefficients have then been estimated in their nonlinear nature using the United States Air Force's *Stability and Control Datcom* methodology (WV76) and the *Digital Datcom* software.

One has to keep in mind that this is only a parameterization of the airflow around the aircraft, not a precise description of it. Especially the effects during stalls and very high angles of attack are difficult to describe using these techniques. Even small angles of sideslip might cause an asymmetric stall during these high angles of attack and would result in a highly asymmetric flight condition. This is especially true for the ensuing analysis of the aggressive winch launch in section 3.2.9.

Also, the analysis of structural effects in this thesis is only of secondary interest. For example, an overspeed of the ASK 21's maximum winch launch speed of $V_W = 150 km/h$ is only looked at when it is excessive.

3 Results

Safety Margin

One of the primary concerns of this thesis is the safety analysis of potential critical situations, as they might occur while winch launching. It is deemed especially critical if the glider reaches a stalled state during the launch process. Because trajectory control precision is insufficient during stalled flight and the glider decelerates quickly towards the stall speed when pitched upwards without an acting cable force, a cable break is one of the worst case scenarios that might occur. Due to this, the relative difference between the aircraft's airspeed V_a and stall speed V_S is defined as the safety margin S.

$$S := \frac{V_a - V_S}{V_a} \tag{3.1}$$

One should bear in mind that the aircraft's stall speed is proportional to the square root of the vertical load factor $n_z = \frac{-Z_a}{m_{\mathrm{AC}} \cdot g}$ and the aircraft's stall speed in steady flight $V_{S,1g}$. The safety margin follows as:

$$S = \frac{V_a - V_{S,1g} \cdot \sqrt{n_z}}{V_a} = 1 - \frac{V_{S,1g} \cdot \sqrt{n_z}}{V_a} \tag{3.2}$$

This also means that the safety margin is an expression for the angle of attack α. If the glider reaches its stalling angle of attack $\alpha_{\mathrm{S}} = 8°$ - which is also the angle of the maximum lift coefficient - then the wing is completely stalled and the safety margin has reached a value of $S = 0$.

3.1 Reference Simulation

To properly evaluate the influences of varying the different simulation parameters, the following simulation conditions have been defined as standard and will serve as the reference launch for further analysis. All simulations are conducted using standard atmospheric values with the aircraft initializing at sea level.

3.1.1 Reference Simulation Settings

General:

- Time step size $\Delta t = 0.01s$

Wind:

- No wind is present in the reference simulation: $(u, v, w)^T_{\mathrm{Wind},g} = (0, 0, 0)^T$

Winch:

- Winch location $(x, y, z)_{W,g}^T = (1000m, 0, 0)^T$

Winch Operator:

- PID winch force controller with time- and glider position-dependant target force
- Initial target winch force $F_{T,0} = 4000N$
- Nominal rate of change of target winch force $\frac{dF_T}{dt} = 500N/s$
- Maximum target winch force $F_{T,\max} = 8000N$

Glider:

- Initial unaccelerated track speeds[1] $(u, v, w)_{k,0}^T = (18.8m/s, 0, 0)^T$
- Initial Euler angles $(\Phi, \Theta, \Psi)_0^T = (0, 0, 0)^T$
- Elevator trim angle $\eta_{\text{Trim}} = -3.0°$
- CG hook location $(x, y, z)_{\text{CG-Hook},f}^T = (0.6m, 0, 0.3m)^T$

Pilot:

- PID airspeed controller and pitch damper engage at safety altitude $h_{\text{Safety}} = 50m$
- Pilot's target airspeed $V_T = 30m/s = 108km/h$ IAS

Cable:

- Synthetic cable with the following physical properties[2]:

Mechanical Property

Diameter	$d_c = 5.0mm$
Mass per Unit Length	$\bar{m}_c = 1.88 \cdot 10^{-2} kg/m$
Modulus of Elasticity	$E_c = 4.025 \cdot 10^{10} Pa$
Strain-speed Stress Coefficient	$c_c = 1.56 \cdot 10^7 Pa \cdot s$

Derived Mechanical Property

Mean Cross Section	$A_c = 19.6mm^2$
Mean Density	$\rho_c = 960kg/m^3$

Aerodynamic Properties

Drag Coefficient	$C_{D,c} = 1.3$

note:
No data was available for the value of c_c. It has been selected in such a way as to notably dampen cable vibration.
Anderson (And07) provides this experimental $C_{D,c}$ value for the two-dimensional viscous flow over a cylinder with $Re = \frac{\rho_0 \cdot v_{\text{ref}} \cdot d_c}{\mu_0} = \frac{1.225 \frac{kg}{m^3} \cdot 30 \frac{m}{s} \cdot 5.0mm}{1.7894 \cdot 10^{-4} \frac{kg}{m \cdot s}} \approx 1.0 \cdot 10^4$.

[1] In no-wind conditions, this is equivalent to the glider's stall speed in undisturbed airflow $V_{S,1g}(m_{\text{AC}} = 510kg) = 18.8m/s$ (Ale80).
[2] Courtesy of Rosenberger Tauwerk GmbH

FEM Model:

- Initial number of elements $n_0 = 20$
- Initial location of elements: equally spaced along straight line between CG tow hook and winch location

3.1.2 Reference Results

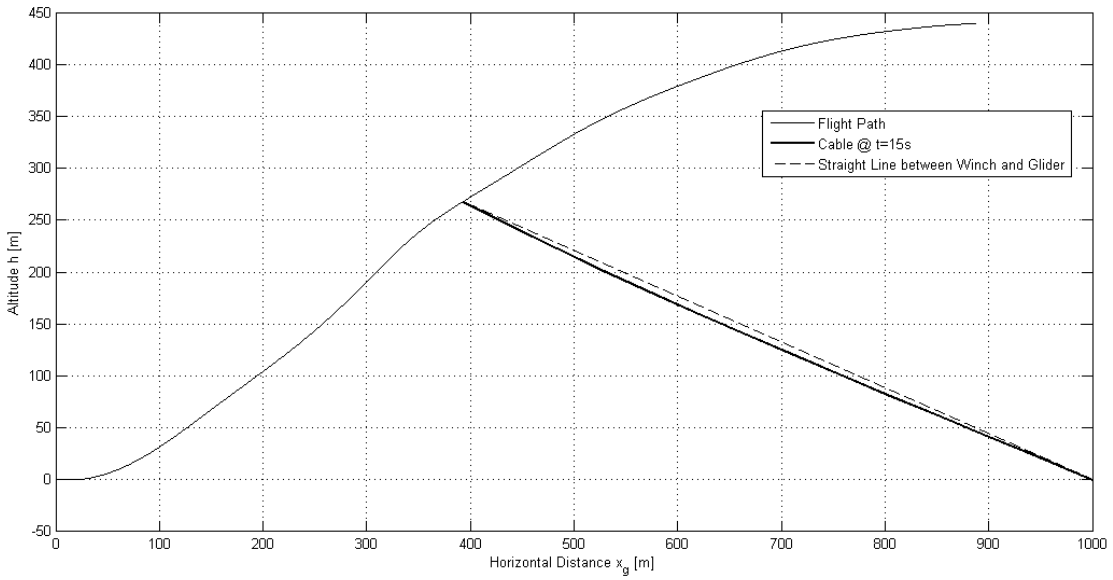

Figure 3.1: Flight Path of the Reference Configuration

The simulation of the reference configuration supplies a flight path of the glider as presented in flight path diagram 3.1. In this case, the glider will reach a release altitude of $h_{\text{Release}} = 439m$ at $t_{\text{Release}} = 33s$. For illustrative purposes, the deformed cable at the moment of $t = 15s$ has been plotted into the mentioned flight path diagram. A cable deflection due to acting external forces can clearly be seen against the connecting straight line between the glider and winch. This deflection seems reasonable and shall serve as partial validation of the cable model.

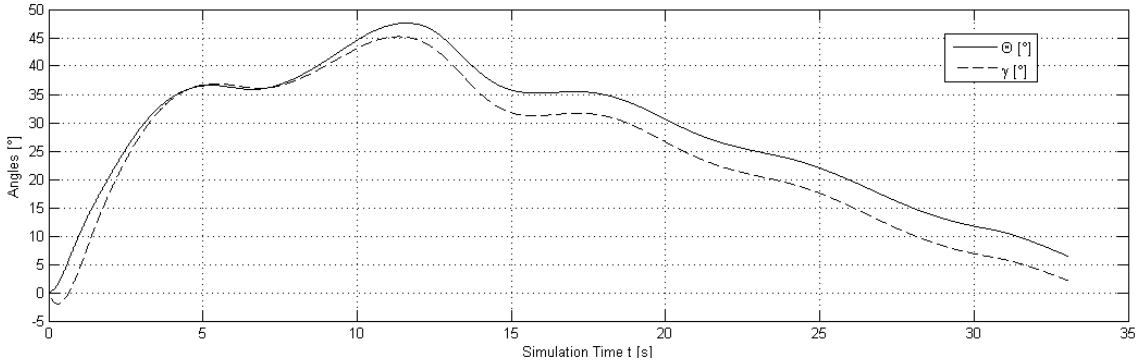

Figure 3.2: Pitch and Climb Angles during Reference Launch

Figure 3.2 illustrates the progression of the pitch angle Θ and climb angle γ during the reference simulation. The initial dip in γ at $t \approx 0.3s$ is due to the aircraft having an insufficient initial angle of attack α_0 at the beginning of the simulation to support its own weight[3].

Especially once the glider has traversed the maximum pitch and climb angles $\Theta_{\max}$ and $\gamma_{\max}$ at $t \approx 11.5s$, a damped phugoid mode becomes obvious. Without the pitch damping function of the `Glider Pilot` block, this phugoid would be more strongly pronounced. Yet in practical flight operations, the damping of the phugoid mode during the winch launch is often dependent upon pilot skill.

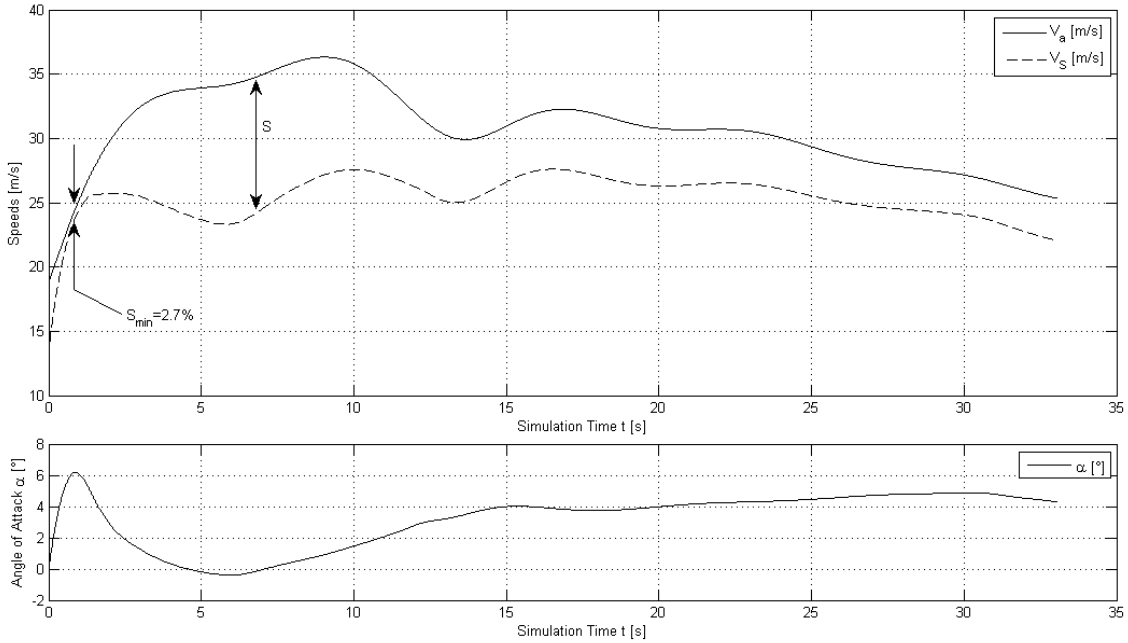

Figure 3.3: Safety-relevant Parameters during Reference Launch

A plot of safety-relevant parameters during the reference winch launch is given in figure 3.3 which also implicitly supplies the safety margin S. The initial peak of the angle of attack α at $t = 0.9s$ corresponds with the decreasing distance between airspeed V_a and stall speed V_S, resulting in a minimum safety margin $S_{\min} = 2.7\%$ at this moment. This is partially due to the glider's descending flight path within the simulation's first second, yet also corresponds with the necessity for rotating into a nose-up attitude for the initial climb. In practical measurements, it is expected that $S_{\min}$ would be larger than the given value, since the aircraft would not have a negative climb angle below ground level. Instead, the glider will continue its ground roll. This serves to lessen the acting angle of attack and decrease the load factor and stall speed, making the actual launch safer in regard to the safety margin S.

As a means of analyzing pilot behavior during the launch, the elevator deflection η is plotted over time in figure 3.4. The pilot will initially hold the elevator in the steady trimmed condition until the safety altitude of $h_{\text{Safety}} = 50m$ is reached at $t_{\text{Safety}} = 4.25s$. This marks the onset of airspeed control which can also clearly be seen in figures 3.2 and 3.3. Airspeed acceleration $\dot{V}_a$ lessens and the controller

[3]Recall that neither a ground effect model nor a ground model has been implemented in the simulation.

pitches the aircraft farther up to approach the target airspeed of $V_T = 30m/s$. Yet, this particular pitch-up motion appears to excite the glider's phugoid mode slightly. During the final phase of the launch, starting at $t \approx 21s$, the pilot eventually releases back pressure on the controls until cable release.

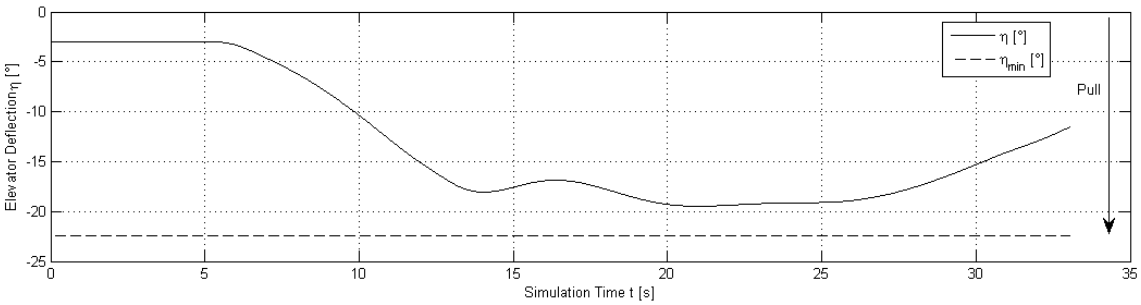

Figure 3.4: Elevator Deflection During the Reference Launch

A plot of the winch force over time, as presented in figure 3.5, shows that the winch operator model performs its task in a satisfying manner. During the first third of the simulation, the operator smoothly increases the winch force $F_{C,W}$ in a steady manner, until at $t \approx 11s$, the maximum winch force is reached. This value is then held nearly constant for the duration of $\Delta t \approx 5s$, when a subtle reduction in the winch force sets in as the glider-winch-angle χ increases. This allows for a smooth transition into steady and horizontal flight by the glider. By time the cable is released, the winch force will have decreased to a value of only $F_{C,G} \approx 2300N$, allowing for only a small change in loads acting on the aircraft and reducing wear on materials.

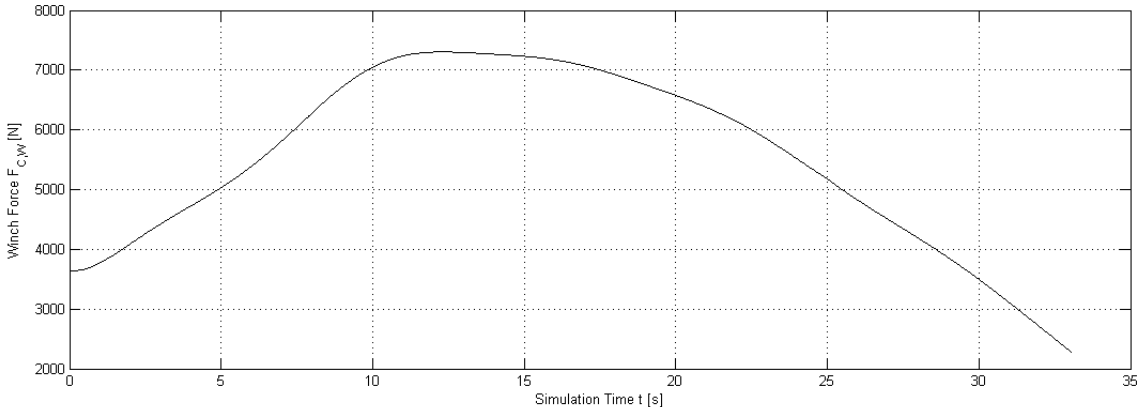

Figure 3.5: Winch Force during the Reference Launch

3.2 Variation of Parameters

To gain a better understanding of the physical occurrences during the winch launch process, the glider's response to changes in certain parameters is analyzed. The results - within the context of the underlying physical and numeric models - are then used to substantiate or rebut several working hypotheses.

3.2.1 Influence of Synthetic vs. Steel Cable

One of the current disputes within the soaring community is the effectiveness of replacing the previously standard steel cables with synthetic ones. A wide range of "personal values of experience" and "empirical values", primarily regarding the gain in release altitude by using synthetic cables, can be heard. This makes a comparison of the cable types within this simulation of interest.

To reach this, the cable properties have been changed to those of a steel cable:

Mean Density	$\rho_c = 4250 kg/m^3$
Modulus of Elasticity	$E_c = 1.70 \cdot 10^{11} Pa$
Strain-speed Stress Coefficient	$c_c = 2.50 \cdot 10^8 Pa \cdot s$

note:
The cable diameter and drag coefficient remain unchanged.
While Dietz and Mupende (DM04) recommend an undamped steel cable model, the above value for c_c has been chosen to provide adequate numeric damping.

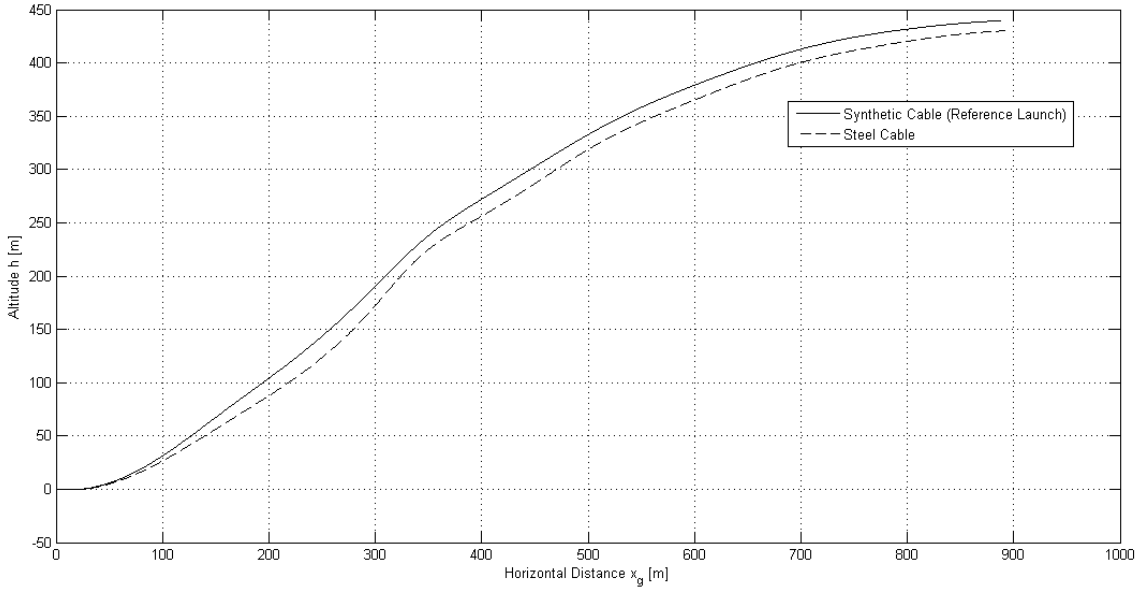

Figure 3.6: Flight Paths with Varying Cable Types

The flight path diagram 3.6 shows a release altitude gain of $\Delta h_{\text{Release}} = 9m$ in favor of the synthetic cable. This result cannot support the claim of the often mentioned "significant gains" by the use of synthetic cables. Yet, their advantages in terms of weight, manageability and splicing shall remain untouched.

3.2.2 Influence of Tow Distance

In the past, winch launching has primarily taken place at general aviation airfields. There, spatial and air traffic restrictions often limit the available towing distance[4] to $d_{\text{Tow}} = 1000m$ or less. However, temporary access of some European operators to

[4]distance between the glider's take-off point and the winch location

larger airfields, often being inactive or little used military or commercial facilities, has brought a rise in interest on longer tow distances. At the same time, the mass increase associated with longer steel cables brought with it some inherent difficulties. The constructive changes in winches necessary to accommodate the increased inertial loads caused by the significant increase in cable mass were long considered to be elaborate. A further hindrance of increasing tow distance was the result. However, with the availability of the much lighter synthetic cables, a study of the effects of a longer tow distance seems appropriate.

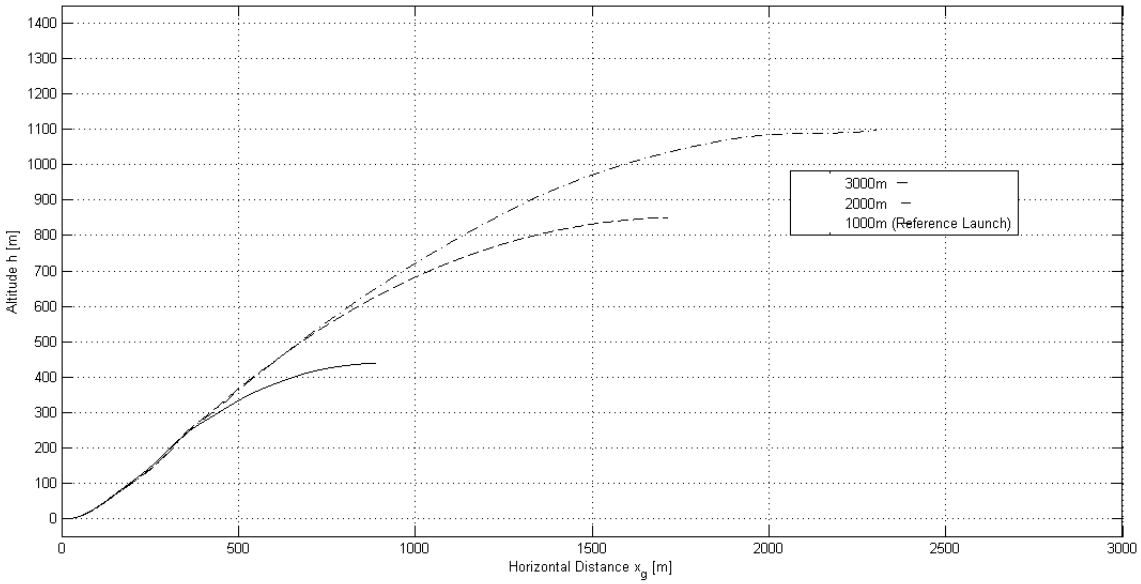

Figure 3.7: Flight Paths with Variable Tow Distance

Release altitudes of $h_{\text{Release}}(d_{\text{Tow}} = 1000m) = 439m$, $h_{\text{Release}}(d_{\text{Tow}} = 2000m) = 851m$ and $h_{\text{Release}}(d_{\text{Tow}} = 3000m) = 1097m$ can be taken from figure 3.7. While the increase in release altitude from the $1000m$ tow distance to $2000m$ is almost proportional, the gain decreases significantly below a proportional value with $3000m$ distance available. This overproportionate decrease might be attributed to winch operator behavior. It is not clear whether an operator would decrease the target winch force in the same manner dependant on the glider-winch-angle χ during a longer tow as during shorter tows. No critical conditions are expected to arise by the increase in tow distance because only the duration during which the cable force $\vec{F}_{G,C}$ acts on the aircraft increases. Its magnitude is expected to remain unchanged. Taking these results, it can be said that at operating locations where longer tow distances are available and useable, the winch launch is a viable alternative to aerotowing.

The significantly higher tow durations with increase in tow distance cause a rise from $t_{\text{Release}}(d_{\text{Tow}} = 1000m) = 33s$ to $t_{\text{Release}}(d_{\text{Tow}} = 2000m) = 63s$ and $t_{\text{Release}}(d_{\text{Tow}} = 3000m) = 85s$. This, together with the notable increase cable retrieve times[5], will lower the maximum winching cadence[6] remarkably.

[5]the time it takes to unreel and lay out the cable between the winch and the launch area
[6]the number of launches that can be conducted within a given span of time

3.2.3 Wind Influence

Whereas the assumption of a no-wind condition in the reference simulation simplifies calculation and estimation and facilitates better compatibility of the data with other works in the field of flight mechanics, it bears only limited significance for actual flight operations. In these, almost always some form of wind and atmospheric movement is present. Two dynamically different cases of wind behavior have been analyzed with the simulation; the case of a steady head- or tailwind and the case of gusts.

Head- and Tailwind

Most flight regulations such as the German "Glider Operation Regulations" (Seg03) limit tailwind glider launch operations to very small values of wind speed or prohibit them completely. Due to this, it was expected that the release altitude of a launch conducted in tailwind conditions would decrease more strongly than that of a launch in an equally strong, yet opposing, headwind.

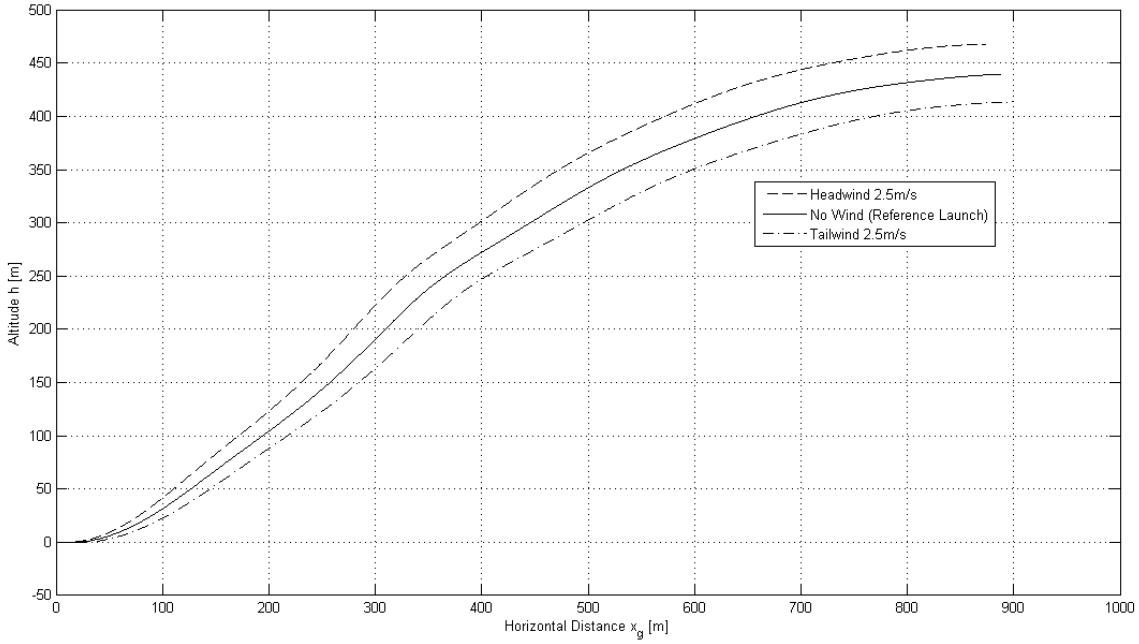

Figure 3.8: Flight Paths with Acting Steady Winds

The simulation results, visualized in flight path diagram 3.8, cannot support this hypothesis. The glider flying in a $2.5m/s$ tailwind will release at $\Delta h_{\text{Release}} = -26m$ below the reference launch and a $2.5m/s$ headwind will cause a gain of $\Delta h_{\text{Release}} = 28m$. Though the safety plot 3.9 for the tailwind condition shows a stalled situation in the interval of $0.6s < t < 1.2s$ where the stalling angle of attack α_S is exceeded slightly, this has to be interpreted cautiously. A more detailed look at the flight path during this interval reveals, that the glider has descended to an altitude of $h < 0m$, due to the lack of a ground model. This cannot be interpreted as being physically meaningful, but much rather should be seen as a continuation of the ground roll. Only once sufficient airspeed is reached will the glider lift off which is expected to occur at a time, when the angle of attack α is again below its stalling

value. To provide a more meaningful safety analysis of the situation during which the glider takes off in a slight tailwind, the inclusion of proper ground-effect and ground models are necessary. However, the increased duration of a lower dynamic pressure acting on the aircraft becomes apparent in figure 3.9. A pilot transitioning into the climb too early - by not properly regarding the decreased airspeed at the beginning of the launch - still runs the risk of stalling the glider. A glider launch in tailwind conditions is safely possible only if the decrease in airspeed is accounted for and the pilot is not distracted by the visual and inertial impressions of a higher groundspeed.

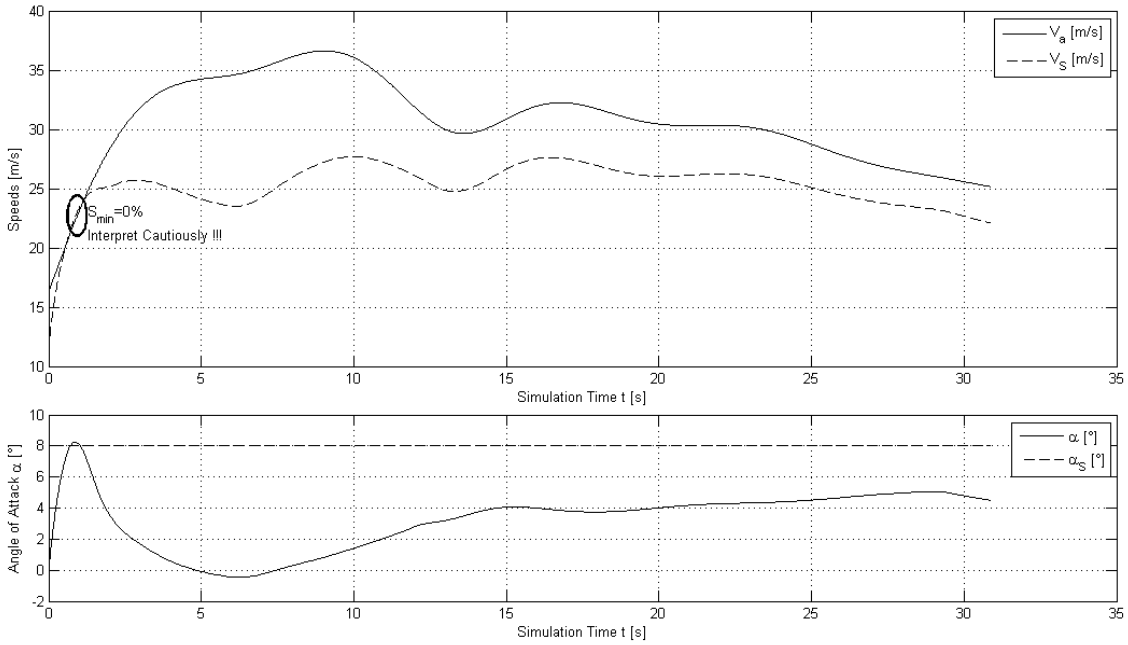

Figure 3.9: Safety-relevant Parameters with $2.5m/s$ Tailwind

This is not to say that tailwind operations are favorable. In fact, one of the most problematic situations for the winch operator is the control and steering of a descending cable and drag chute that is being blown towards the winch and runs the risk of passing it. Also, traffic coordination between landing and departing aircraft becomes more challenging in this situation and emergency procedures such as in the event of a cable break, are also influenced. The results should much rather be interpreted as overly rewarding launch operations with a headwind component.

Gust Response

Contrary to the preceding analysis of flight paths in windy conditions, the primary concern of the gust analysis is to determine and describe the response of the cable and not the aircraft's trajectory. The simulation is exposed to both, an instant headwind gust and an instant updraft gust. The magnitude of each gust is $2.5m/s$ and acts for the duration of $t > 9s$. In the case of the $2.5m/s$ headwind gust, the glider is exposed to the wind function

$$(u, v, w)^T_{\text{Wind},g} = \begin{cases} (0,0,0)^T & t < 9s \\ (-2.5m/s, 0, 0)^T & t \geq 9s \end{cases} \tag{3.3}$$

and the $2.5m/s$ upwind gust is described by the wind function

$$(u,v,w)^T_{\text{Wind},g} = \begin{cases} (0,0,0)^T & t < 9s \\ (0,0,-2.5m/s)^T & t \geq 9s \end{cases} \tag{3.4}$$

As a measure of cable response, the weak link force[7] $F_{G,C}$ has been chosen.

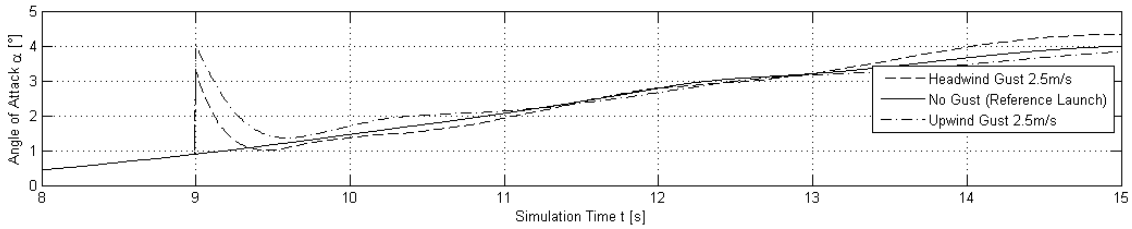

Figure 3.10: Angle of Attack during Gusts

Figure 3.10 reveals that the updraft gust causes a stronger increase in the angle of attack α at the instant of gust onset than the headwind gust does. Even though the upwind gust appears to be more critical, no safety analysis is performed. An updraft gust of this magnitude is not expected to develop in close proximity to the ground because the airflow is restricted to primarily horizontal movement by the ground, making a stall unlikely. The statically stable configuration of the ASK 21 causes the glider to respond with a pitch-down moment in the upwind gust case, but the aircraft's airspeed is increased more by the headwind gust. This is responsible for the slight pitch-up motion of the glider following the headwind gust, as can be seen in figure 3.12. These are classic excitations of the phugoid mode in the aircraft's longitudinal motion.

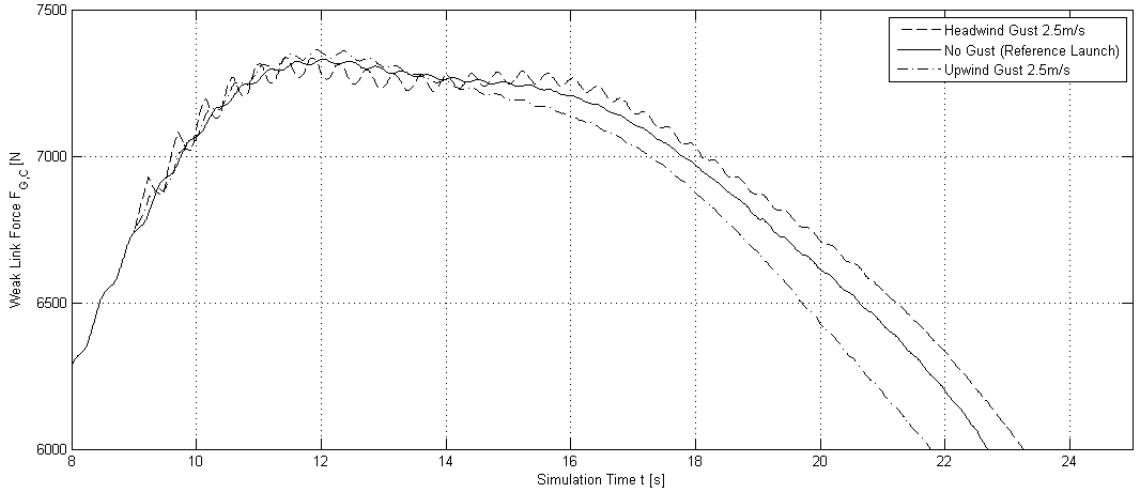

Figure 3.11: Weak Link Force Response after Gust Disturbance

Each response of the weak link force in figure 3.11, to either the vertical or horizontal gusts, can be interpreted as an overlay of a higher frequency oscillation with

[7]Since the weak link sits close to the glider end of the cable, it is said that the weak link force is the absolute value of the force exerted by the cable onto the glider.

a small amplitude and a lower frequency oscillation with a larger amplitude. Both higher frequency oscillations have a frequency of $f_{\mathrm{hf}} = 2.5Hz$ and appear to be well damped. These are therefore attributed to physical and numeric oscillation of the cable due to a change in mean cable tension caused by the gusts. Their amplitudes are of up to $T'_{1,\mathrm{hf}} \approx 30N$ for the headwind gust and $T'_{1,\mathrm{hf}} \approx 20N$ for the horizontal gust. These values are comparatively low and the danger of overstressing the cable due to these higher frequency vibrations is considered to be low. For future experiments, it is expected that the amplitude of the higher frequency oscillations will increase and gain more relevance for aircraft with lower wing loading as they are more susceptible to gusts.

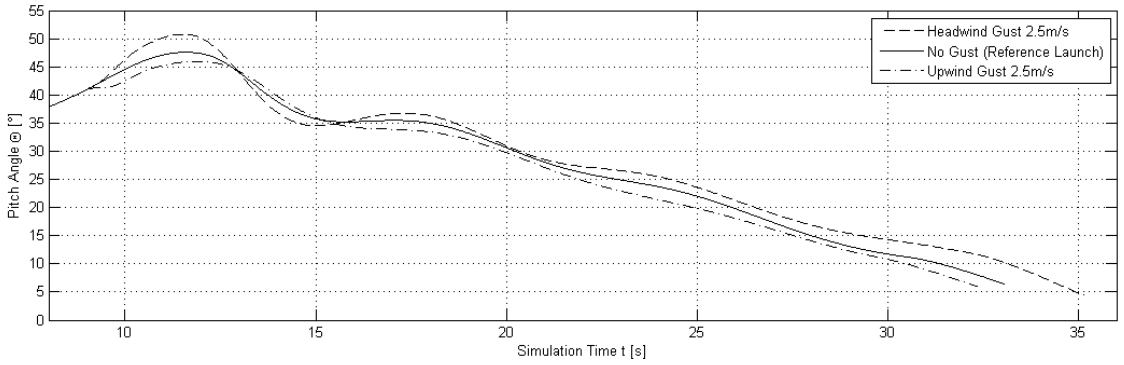

Figure 3.12: Changes in Pitch due to Gusts

In the case of the calculations performed with the ASK 21 the lower frequency oscillations in weak link force dominate, having a frequency of $f_{\mathrm{lf}} = 0.2Hz$. This matches the phugoid's frequency very well, as can be seen in figure 3.12, and causes the low frequency changes in cable load to be attributed to changes in the aircraft's flight path. This oscillation's amplitude can be much larger in certain cases such as a stronger gust and might exceed the equivalent value of the weak link force in the reference condition. An accidental overload of the cable, exceeding the weak link breaking strength, seems more likely in this case.

3.2.4 Influence of Tow Hook Location

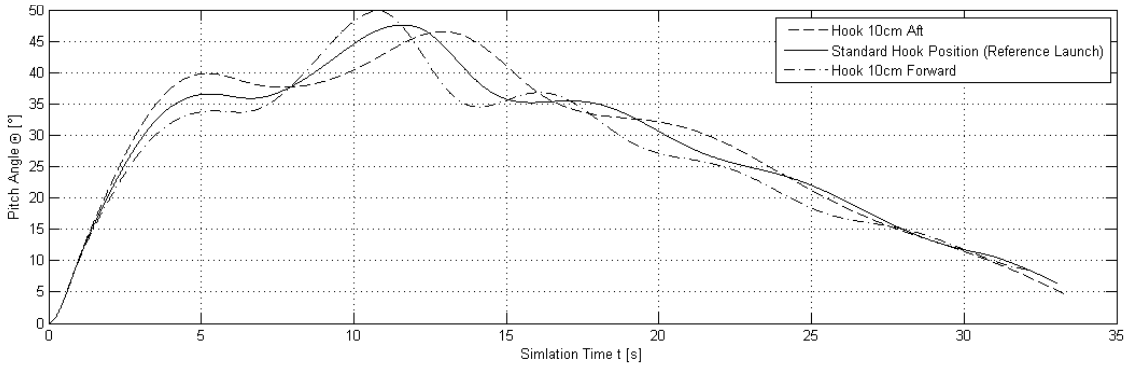

Figure 3.13: Changes in Pitch due to Tow Hook Location

Another goal of this thesis is to gain a qualitative understanding of the influence the mounting location of the CG hook has on the glider's launching behavior. Since the hook is mounted closely to the CG, and the cable force induced into the hook is of larger magnitude than the aircraft's weight, even small alterations in the moment arm are expected to significantly modify the aircraft's longitudinal motion behavior. For the comparison of mounting positions, the hook location was moved $10cm$ forward of the reference condition's location to $(x, y, z)^T_{\text{CG-Hook},f} = (0.7m, 0, 0.3m)^T$ and $10cm$ aft to $(x, y, z)^T_{\text{CG-Hook},f} = (0.5m, 0, 0.3m)^T$.

The plot of figure 3.13 shows that the aft mounted hook causes slightly higher pitch angles in the first and later phases of the launch than the reference condition or the forward mounted hook. However, the maximum pitch angle decreases from $\Phi_{\text{max, forward}} = 50°$ and $\Phi_{\text{max, ref}} = 48°$ to $\Phi_{\text{max, aft}} = 47°$. A more docile phugoid mode for the aft mounted hook is one of the consequences, while also providing a release altitude gain of $\Delta h_{\text{Release}} = 0.2m$ to the reference condition. At the same time, the forward mounted hook has a release altitude loss of $\Delta h_{\text{Release}} = -1.2m$, as shown in flight path plot 3.14. These changes are only menial and it is doubted that these could be effectively proven in flight tests due to the numerous other perturbations acting on the aircraft.

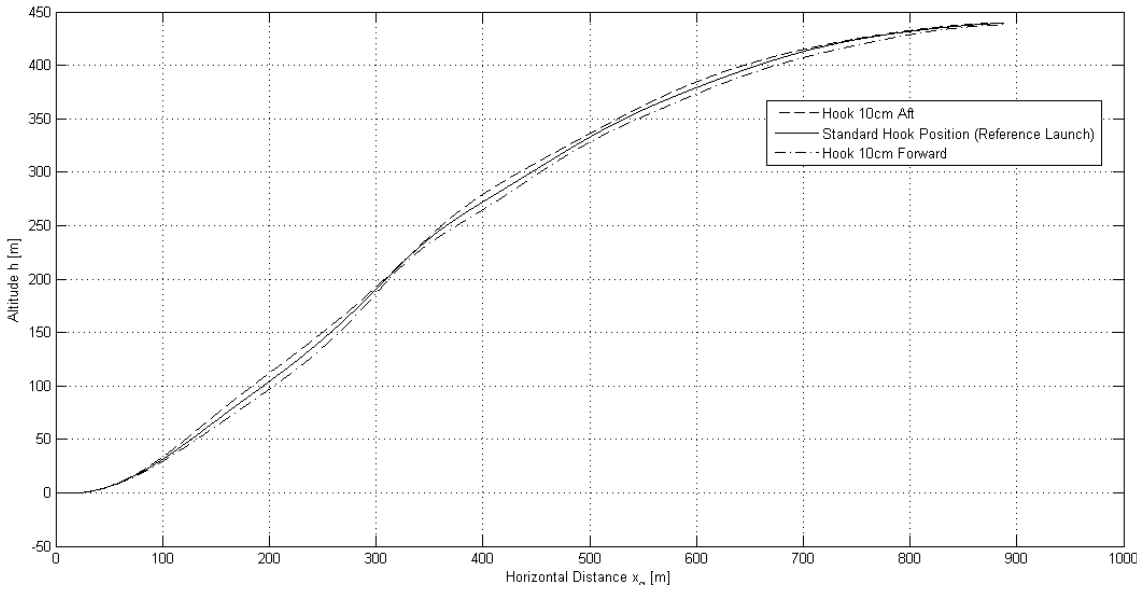

Figure 3.14: Influence of CG Hook Location on Flight Path

The higher pitch angles in the initial climb phase, caused by the tow hook being in the aft position, make a safety analysis of this configuration highly recommendable. Yet figure 3.15 shows a decrease of the safety margin from $S_{\text{min}} = 2.7\%$ in the reference launch to $S_{\text{min}} = 2.5\%$ in the configuration with a farther aft CG hook. This is only a very marginal decrease and is opposed by the reduction in pilot workload due to the more favorable longitudinal motion modes of this configuration.

In light of these results it can be said that there is still potential for flight mechanically optimizing the location of the CG tow hook of the ASK 21 training glider. But at the same time, further analysis is necessary to properly evaluate the feasibility of such a design change. Particularly, the structural modifications necessary

as well as the changes in handling quality need to be assessed. At last, the question of how other aircraft might respond to the same design changes is of interest. It is considered likely that other gliders also have further development potential in their designs to increase launch performance.

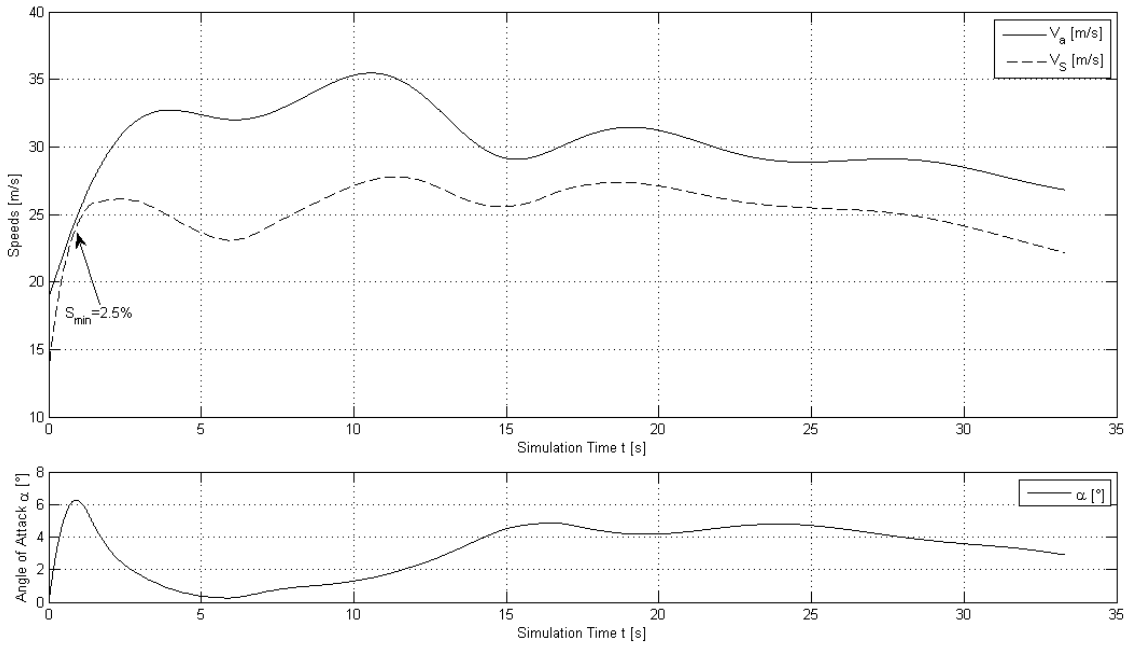

Figure 3.15: Safety-relevant Parameters with CG Hook Moved 10cm Aft

3.2.5 Influence of Winch Operator Behavior

One of the main differences in operator behavior is how fast the operator advances the winch throttle to the final target setting. Since the winch throttle is controlled via the winch force by the `Winch Operator` block, the nominal rate of change in winch target force $\frac{dF_T}{dt}$, is taken as a means of modifying winch operator behavior.

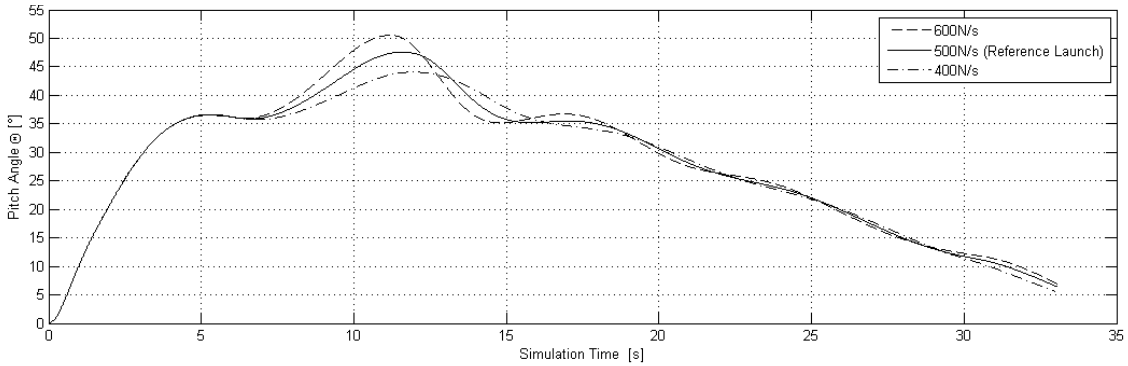

Figure 3.16: Changes in Pitch due to Operator Behavior

The time-pitch-plot in figure 3.16 readily shows that even small changes of $\frac{dF_T}{dt}$ notably change the longitudinal stability of the aircraft during the launch process. A decrease in the rate of change of the target winch force will lessen the phugoid amplitude while an increase will strengthen it. The obvious consequence for the pilot is that the workload will increase when the winch throttle is opened more swiftly.

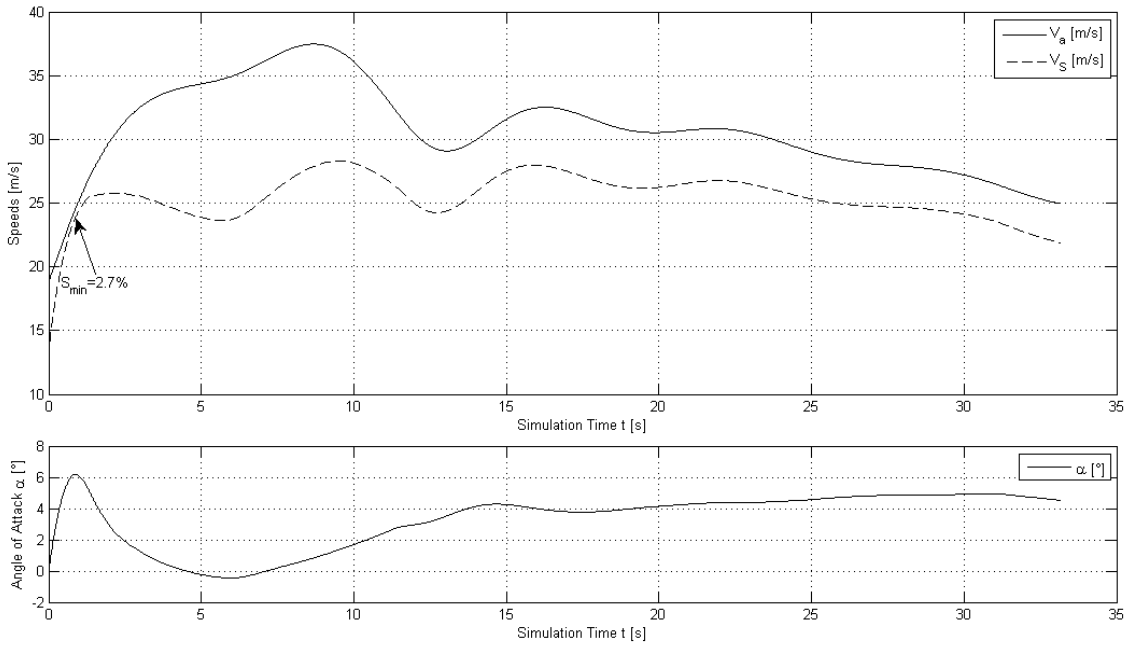

Figure 3.17: Safety-relevant Parameters for Nominal Winch Target Force Rate of Change $\frac{dF_T}{dt} = 600N/s$

This increase in workload, along with the fact the winch force $F_{C,W}$ is higher during the early parts of the tow[8], is expected to make an increase in $\frac{dF_T}{dt}$ more

[8] An increase in the winch force $F_{C,W}$ results in higher pitch-up moments.

critical. Yet, figure 3.17 reveals that even a 20% increase of $\frac{dF_T}{dt}$ to $\frac{dF_T}{dt} = 600N/s$ from the reference simulation value of $\frac{dF_T}{dt} = 500N/s$ causes no notable change in the minimum of the safety margin $S_{\min}$. It remains at a value of $S_{\min} = 2.7\%$. The release altitude does not seem to vary much either, as shown by figure 3.18. Only a release altitude gain of $\Delta h_{\text{Release}} = 4m$ is apparent by the 20% increase in $\frac{dF_T}{dt}$, while the same absolute decrease causes only a release altitude loss of $\Delta h_{\text{Release}} = 5m$. In general, it seems that the effects of a change in $\frac{dF_T}{dt}$ are only minor on the release altitude and safety margin. But the swifter raising of the winch target force appears to require more of the pilot's attention.

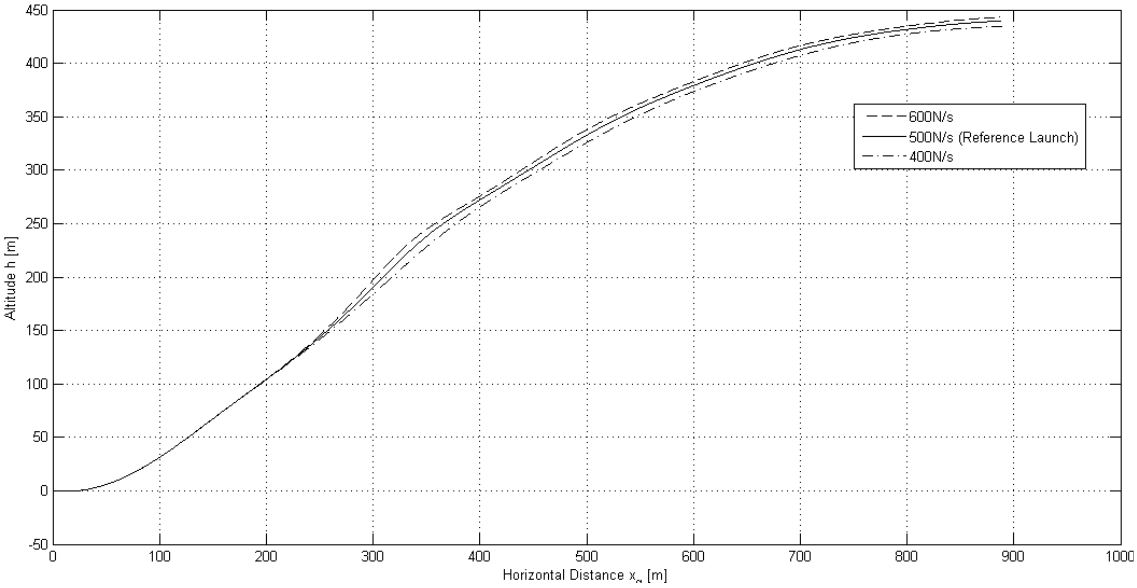

Figure 3.18: Flight Paths with Varying Target Force Rate of Change $\frac{dF_T}{dt}$

3.2.6 Winch Force Influence

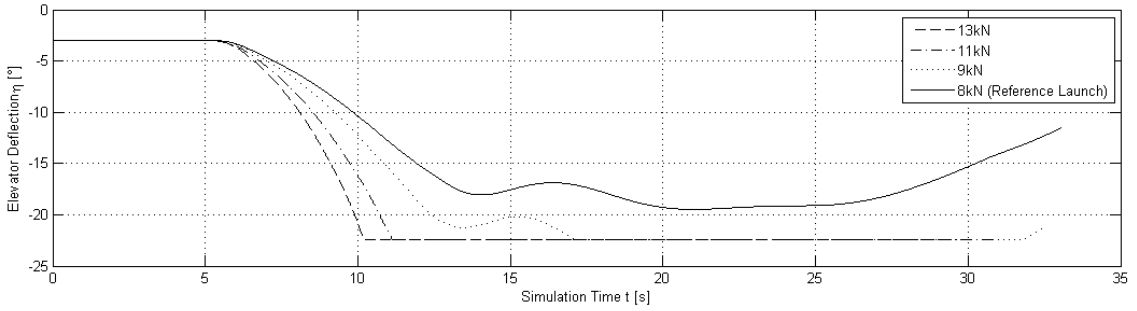

Figure 3.19: Elevator Deflection η with Varying Maximum Target Forces $F_{T,\max}$

An obvious way to increase release altitude is to increase the winch force $F_{C,W}$. This higher winch force has been achieved by varying the winch operator's final target winch force $F_{T,\text{final}}$. The time during which the target force is increased from the constant initial value of $F_{T,0}$ has also been held constant, causing a variation in the

nominal rate of change in winch target force $\frac{dF_T}{dt}$. Also, the upper limit of $F_{T,\text{final}}$ is defined by the maximum attainable torque of the engine.

An increase in release altitude of $\Delta h_{\text{Release}} = 63m$ between the reference simulation ($F_{T,\text{final}} = 8kN$) and a maximum target force of $F_{T,\text{final}} = 13kN$ is seen in flight path plot 3.20 of this numeric experiment. This value of $F_{T,\text{final}} = 13kN$ is close to the maximum engine torque of $T_{E,\text{max}} = 895Nm$, corresponding to a winch force of $F_{C,W,\text{max}} = 13.15kN$. The difference between $F_{T,\text{final}} = 13kN$ and $F_{C,W,\text{max}} = 13.15kN$ is said to be a necessary operational reserve for operations out of the engine's optimal working point.

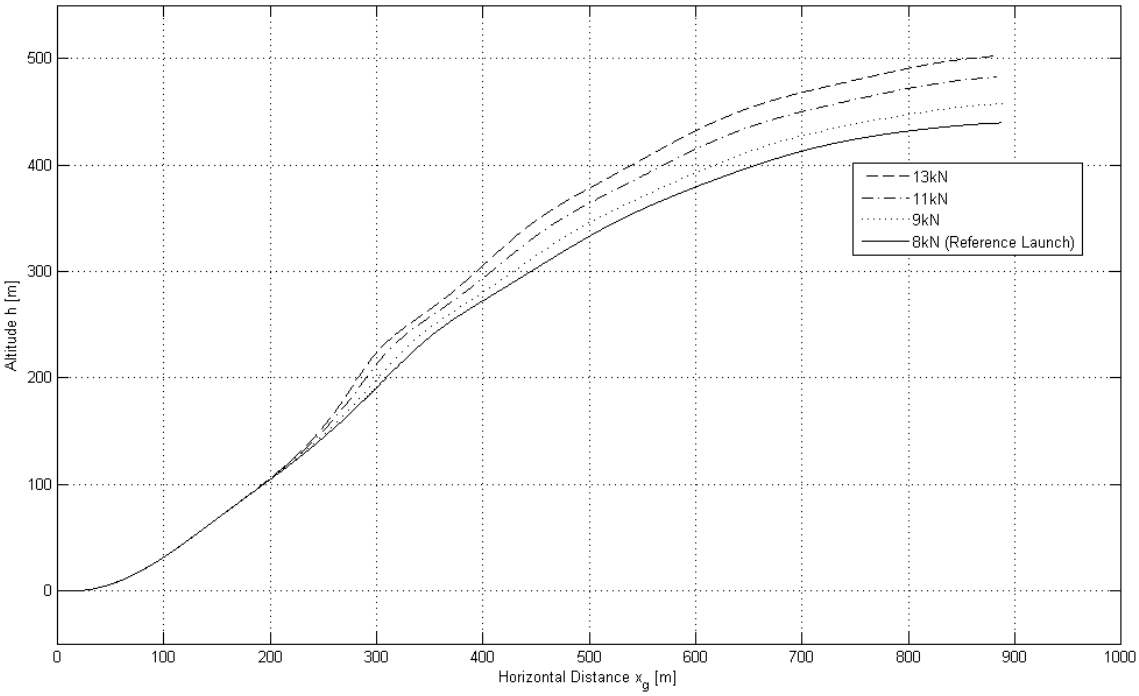

Figure 3.20: Flight Paths with Varying Maximum Target Force

Operations with increased cable forces also bear some inherent risks. The weak link breaking strengths need to be increased, thereby exposing the glider to higher loads, induced at the CG hook. Currently, the ASK 21's pilot operating handbook (Ale80) allows for a maximum weak link breaking strength of $10000N \pm 1000N$ for winch launches, making structural strengthening mandatory for the simulated increases in target and cable forces. At the same time, figure 3.19 shows that even with a maximum target force of $F_{T,\text{max}} = 9000N$, the pilot will hold the controls in the full aft position for most of the tow duration. This situation is aggravated by a further increase in the maximum tow force $F_{T,\text{max}}$ and it is expected to cause an uncompensated increase in airspeed due to the limited flight control authority.

A further area of concern was that the vector of the cable induced tow force $\vec{F}_{G,C}$ is directed almost orthogonally downwards to the flight path during the later phase 5 of the winch launch. At the same time, the magnitude of $\vec{F}_{G,C}$ has been significantly increased by raising $F_{T,\text{max}}$ and $F_{C,W}$. This large downwards-directed force requires a significant increase in lift and load factor for the aircraft to hold its altitude or continue to climb. During this, the pilot is unaware of an increase in load factor, since the aircraft does not accelerate in the z_a-direction. It has been

thought possible that the aircraft approaches a stall in this configuration and that was the reason - along with the potential increase in airspeed - for a further safety analysis of this specific launch configuration. The maximum target winch force of $F_{T,\max} = 13kN$ has been determined to be the most critical case of the conducted numeric experiments.

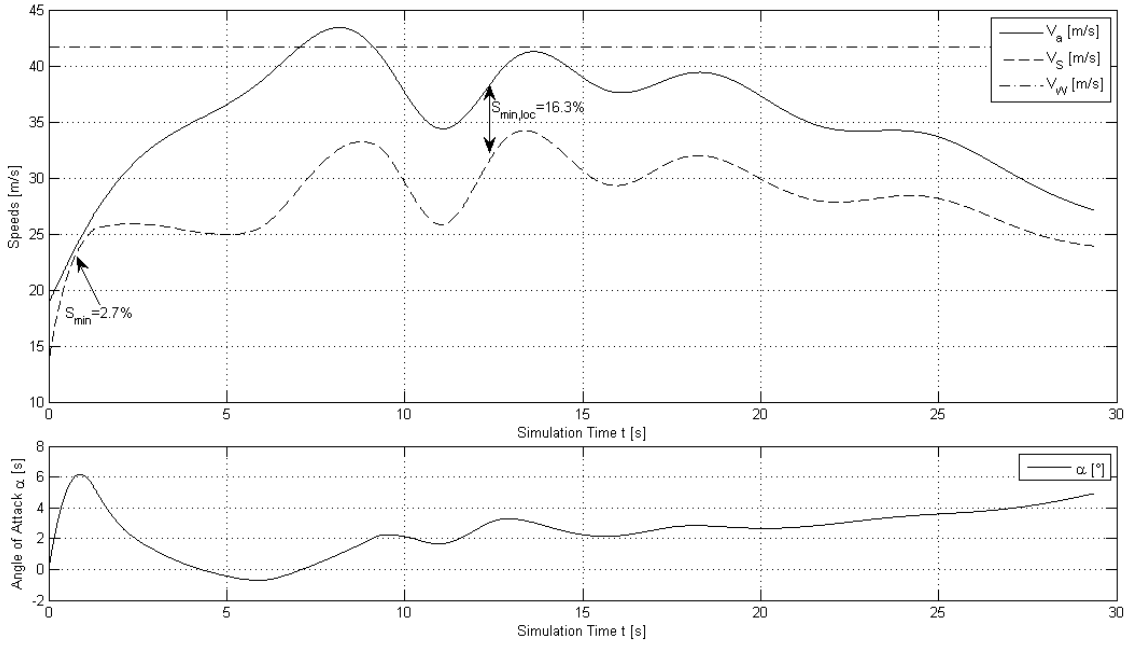

Figure 3.21: Safety-relevant Parameters for Maximum Target Force $F_{T,\max} = 13kN$

Since the initial target force of $F_{T,0} = 4kN$ is the same as during the reference launch, the safety parameter has the same initial minimum of $S_{\min}(t \approx 1s) = 2.7\%$ as during the reference launch. During the second half of the winch launch, when the increased winch force has reached its maximum influence, the safety parameter drops to a further local minimum of $S_{\min,\mathrm{loc}}(t \approx 13s) = 16.3\%$. While this shows that a sufficient margin to the stall is being held in this launch configuration, it is obvious by the variations in airspeed that the limited elevator authority makes airspeed control difficult for the pilot. Even though the ASK 21's maximum winch launch speed (Ale80) of $V_W = 150km/h = 41.7m/s$ is briefly exceeded by $1.7m/s = 6.1km/h$, it is expected that this is not structurally critical and that there is development potential in the ASK 21's airframe for a structural solution. It is also supposed that a strengthening of aircraft's primary structure is possible to support the increase in loads acting on the tow hook. Under these structural assumptions, the presented results support the thesis that a notable increase in tow force can raise release altitudes by a significant margin.

3.2.7 Influence of Cable Model

In an attempt to gain a more detailed understanding of the physical mechanisms governing the influence of the tow cable on the release altitude of the glider, the standard model presented in section 2.1.3 was modified. Particularly, the flight

paths of the following cable models have been determined and are presented in the flight path diagram 3.22:

FEM with Tension, Gravity and Drag is the model described in section 2.1.3 and regards all presented inertial, internal and external forces.

FEM with Tension and Drag, no Gravity selectively disregards the influence of gravity as it would act on the cable while retaining the effects of internal and inertial forces and aerodynamic drag.

FEM with Tension and Gravity, no Drag selectively disregards the influence of aerodynamic drag on the cable.

FEM with Tension, no Gravity and Drag completely disregards the external forces acting on deforming the cable. Cable deformation is only due to internal and inertial forces.

Secant Model is the physical limit case of a massless ideal cable without aerodynamic drag. It is reached by orienting the winch force along a connecting straight line between the winch an the glider's CG hook.

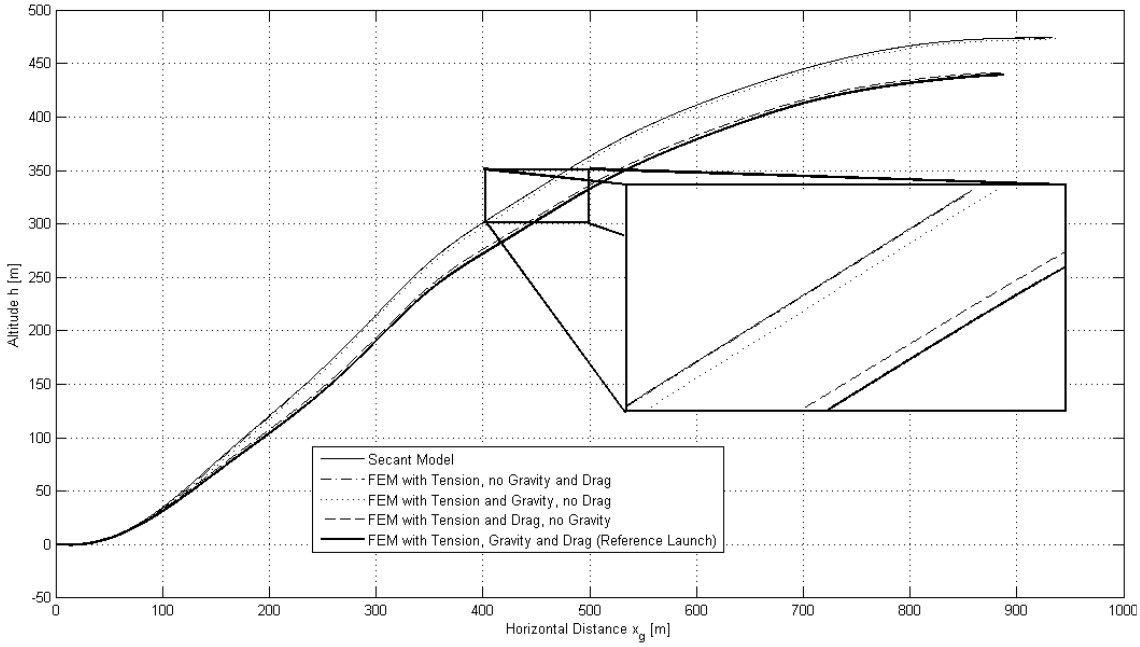

Figure 3.22: Influence of Different Physical Cable Models on Flight Path

The flight path plot of figure 3.22 shows two distinct sets of flight paths, the changing influence between the sets being the aerodynamic drag. At the same time, the flight paths regarding gravity lay below the corresponding flight paths without gravitational influence on the cable. This said, it can be estimated that the gravitational influence causes a release altitude loss of $\Delta h_{\text{Release}} \approx -2m$ whereas the drag influence is $\Delta h_{\text{Release}} \approx -32m$. It is peculiar to note that the flight paths of the ideal **secant model** and the **FEM with tension, no gravity and drag** model are identical for all practical purposes. These negligible differences in the

trajectory serve to show that the inertial forces acting on the cable in the launch are also negligible.

Several development impulses can be drawn from the presented influence of cable models. On the numeric side, the development of a modified secant model with drag and gravitational influence might be favorable. The above mentioned tendencies show that a good correlation between this new model and the reference model might be achieved, while significantly reducing the numeric complexity and increasing the stability of the current algorithms. At times, the occurring numeric instabilities have restricted the use of the cable model of section 2.1.3. Also, the assumption of section 2.1.3, which states that the rendered cable power is negligible, should be challenged. The effect that the aerodynamic cable drag has on the attainable release altitude seems too large to neglect this part of the energy balance.

It is evident that drag seems to more directly influence the cable than gravity does. This is also supported by the change in release altitude that was presented in section 3.2.1. The introduction of synthetic cables into winch launching has primarily modified the cable material density while the cable cross section remains circular to oval with similar diameters to the steel cable. For the future, it is thought to be likely that more prominent gains in release altitude will be reached by reducing the cable diameter and causing lower aerodynamic cable drag. This, however, can only be realized with the availability of cable fibers able to withstand the higher tension in the cable caused by a reduced cross section.

3.2.8 Influence of Cable Drag Coefficient

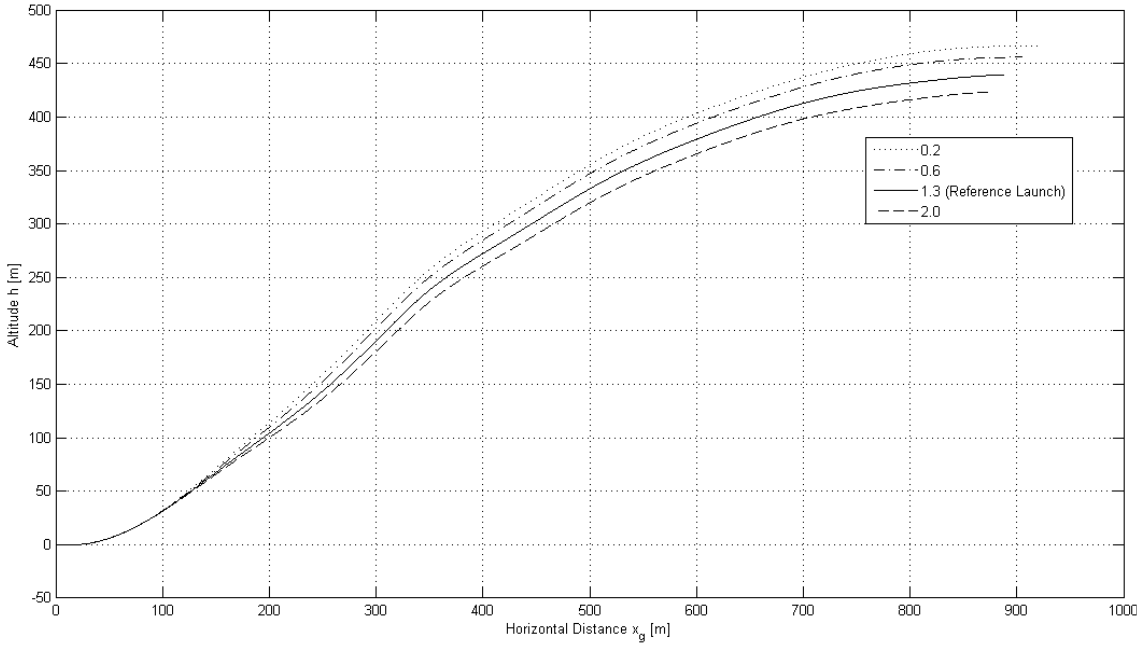

Figure 3.23: Flight Paths with Varying Cable Drag Coefficient $C_{D,C}$

The previous section 3.2.7 identifies the aerodynamic drag acting on the cable as one of the primary influences on release altitude h_{Release}. Since the cable drag coefficient $C_{D,C}$ has so far been estimated and the cable drag model assumes that the cable

is a smooth cylinder, the questions of the susceptibility of the launch behavior to changes in drag arises.

Figure 3.23 shows that a drag reduction of 54%, from $C_{D,C} = 1.3$ in the reference launch to $C_{D,C} = 0.6$, results in an release altitude gain of $h_{\text{Release}} = 17m$. This is almost twice as much as has been gained by the change from a steel cable to a synthetic one. If cable fibers are available that support a significant reduction of the cable diameter safely, then it is expected that the lower drag will cause a notable increase in release altitudes in actual flight operations.

3.2.9 Analysis of Aggressive Pilot Behavior

While so far, no highly critical situations in winch launching have been discussed, the benefit and risks associated with an aggressive winch launch[9], as performed by some pilots, has also been looked at. During such an aggressive winch launch, the pilot will pitch the glider to a steep pitch angle while still in close proximity to the ground, intending to maximize the altitude gain. Before the launch, he or she will usually have placed the elevator trim in an aft position.

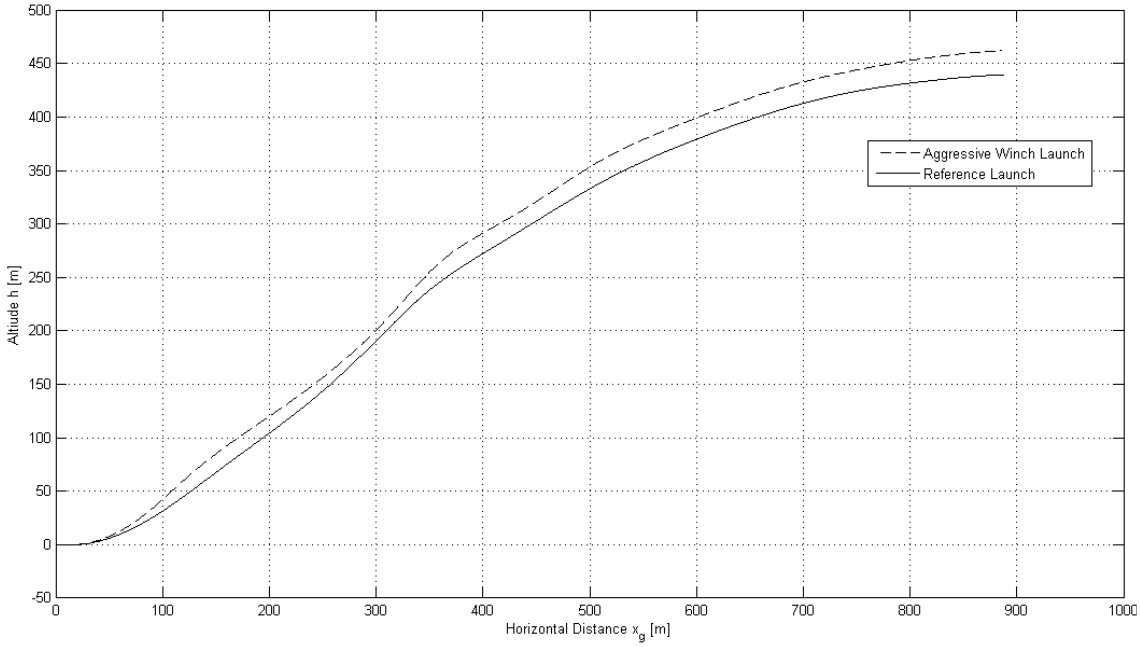

Figure 3.24: Flight Path of Aggressively Flown Winch Launch

To allow for this maneuvering, the safety altitude has been set to $h_{\text{Safety}} = -10m$, causing the `Fading Unit` to experience the unit step already during the simulation's first iteration. This setup allows for the higher rotating speeds in the pitch axis necessary to reach the higher pitch and climb angles early. At the same time, the pilot already begins to track and control airspeed close to the ground. Both of these behaviors are thought to be adequate representations of actual aggressive pilot behavior. Also, the elevator trim angle has been set to $\eta_{\text{Trim}} = -7.0°$, corresponding to approximately 1/3rd aft stick position.

[9] This is the German colloquial "Kavalierstart".

The altitude gain brought by this behavior is plotted in figure 3.24 and has a value of $\Delta h_{\text{Release}} = 22m$. Especially the higher climb gradient close to ground level is prominent in the plot where the flight paths of the reference launch and the aggressive launch quickly diverge.

A comparison of the airspeed and stall speed clearly discloses the risk associated with this pilot behavior. Figure 3.25 shows that during the time frame of $0.7s < t < 1.3s$ the stall speed and airspeed coincide. In the same interval, the stalling angle of attack $\alpha_S = 8°$ is exceeded. This causes the safety margin to shrink to a value of $S = 0\%$ during this interval.

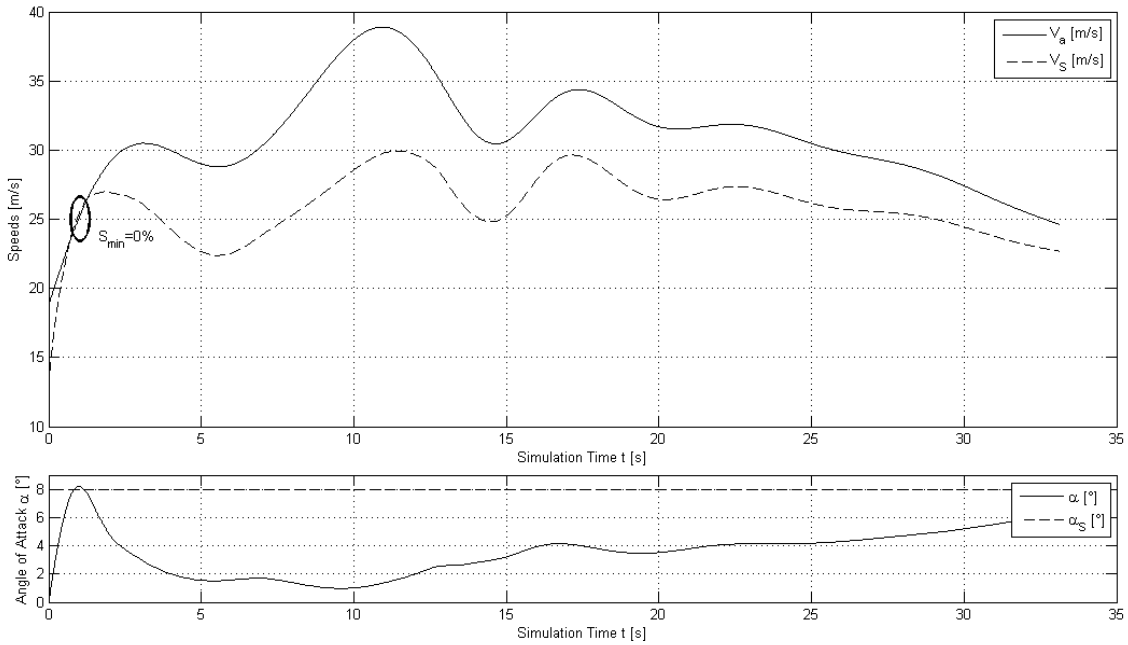

Figure 3.25: Safety-relevant Parameters during an Aggressive Winch Launch

While flight path plot 3.24 shows that the glider will climb at a steeper angle during the initial climb phase when the pilot flies the winch launch aggressively, diagram 3.25 reveals that the glider is actually stalled during this flight phase and illustrates how risky this maneuver is. In the event of a cable break during or near the stall, the aircraft would immediately pitch down, as defined by its natural stability. Yet, the altitudes at which this might occur are more than insufficient for recovery and the glider is expected to crash uncontrollably into the ground. The inherent risk of loss of hull, and more importantly the risk of loss of life of the crew, is obvious.

4 Summary and Outlook

The simulation presented in this thesis illustrates some of the basic mechanisms governing the winch launch as it is practiced at many gliding sites worldwide. Whereas several comprehensive cybernetic models have been coupled in this simulation, areas still in need of improvement within each model have been pointed out for future enhancements. Results could be improved by including an aerodynamic ground effect model and properly modeling the ground to carry the glider and cable. Friction of the ground against the glider and cable should also be modeled in the future. More detailed aerodynamic data on the behavior of the glider in stalled flight needs to be implemented to strengthen the expressiveness of the performed safety analyses. It should also be attempted to gain data of actual winch types and depict a more modern driveline setup regarding a torque converter and other similar equipment and regard the effects of density altitude on engine performance. The numeric difficulties having limited the minimum cable segment length need to be analyzed and solved to improve cable resolution. In the future, the virtual winch operator and pilot behavior need to be compared to actual human behavior. Enhancements of the control laws might regard aspects of fuzzy logic or adaptive control. Also, the enhancement of the simulation to include humans in the loop is thought to be possible.

While the general operationability of winch launches has been proven in practice for several decades, it is also supported by the presented results. It has also been shown that the current methods of winch launching have found an acceptable compromise between performance and safety as no highly critical situations have been found in the reference launch. The existing regulations on tailwind operations are supported by the presented data and gusts seem to have little effect on the weak link force, considering the given wing loading. The destabilizing effect of a quick opening of the winch throttle on the glider's phugoid mode is shown, as well as the possibility of optimizing the tow hook location. Increases in release altitude are gained through changes in the cable type, tow distance and the maximum winch force. While studying the influence of different physical forces on the cable, by varying the cable models, aerodynamic cable drag is identified as another major influence on release altitude, and is analyzed further by varying the drag coefficient. At last, the dynamics of an aggressively flown launch is looked at and the results are in unison with the focus of current training curricula.

It is hoped that the results will provide an impulse for future technical development of winches, gliders and cables. For pilots the analysis of the highly critical aggressive pilot behavior during winch launching hopefully serves to sensitize about the inherent risks of this maneuver and how it can be reduced.

A Coordinate System

In accordance with the general conventions of flight dynamics, several different coordinate systems are used to allow a simple description of the different loads and their sources. The different coordinate systems are all cartesian and are described as follows:

aerodynamic *suffix a*

location of origin: glider CG

axis	indicated direction
$\vec{x}_a$	into the direction of the free slipstream
$\vec{y}_a$	orthogonal to $\vec{x}_a$ and $\vec{z}_a$
$\vec{z}_a$	in the aircraft's plane of symmetry

note: intended for description of aerodynamic loads

aircraft-fixed *suffix f*

location of origin: glider CG

axis	indicated direction
$\vec{x}_f$	longitudinal axis of glider towards primary direction of flight
$\vec{y}_f$	lateral axis of glider towards right-hand side (viewed in primary direction of flight)
$\vec{z}_f$	orthogonal to $\vec{x}_f$ and $\vec{y}_f$

note: simple description of location of aircraft assemblies (e. g. tow hook)

geodetic *suffix g*

location of origin: aircraft's position at initialization of simulation, projected in direction of gravitational acceleration to sea level

axis	indicated direction
$\vec{x}_g$	true north
$\vec{y}_g$	true east
$\vec{z}_g$	direction of gravitational acceleration

Altitude $h = -z_g$

note: simple consideration of gravitational effects, system of choice for description of winch cable

track-fixed *suffix k*

location of origin: glider CG

axis	**indicated direction**
$\vec{x}_k$	direction of track speed
$\vec{y}_k$	horizontal plane
$\vec{z}_k$	orthogonal to $\vec{x}_k$ and $\vec{y}_k$

note: intended for description of inertial forces

For further details on these coordinate systems and their appropriate implementation refer to Brockhaus (Bro01). Note that the transformations between the aircraft-fixed and aerodynamic systems are linear, whereas transformations between any of the aforementioned coordinate systems and the geodetic system are affine due to the spatial separation of the points of origin.

B User's Guide

The following is a brief description of how to operate the winch launch simulation properly. As the different scripts will access data from specific files, it is important to follow the described steps in the proper order. All values are to be entered in *metric units*.

1. OPEN the *Trimmpunkte/WinchLauch.mat* file in the *Trimmpunkte* folder. VARY the initial state of the glider as necessary. The nomenclature used in the file is the same as in (All05). Afterwards SAVE and CLOSE the file.

2. OPEN the *WindVectorField.m* script in the simulation's main directory. Define a time-variant three-dimensional description of the acting wind in *geodetic coordinates*[1]. Then SAVE and CLOSE the file.

3. OPEN the *WinchSimulationParameters.m* script in the simulation's main directory. ALTER all necessary parameters for the glider, pilot, winch, winch operator and cable models. Afterwards, SAVE and EXECUTE the script[2]. Now CLOSE the file.

4. OPEN and EXECUTE the *simgui.m* script in the simulation's main directory. This will launch the simulation's GUI.

5. DEFINE the *simulation duration*[3] (German: "Simulationsdauer") and the *time step size* (German: "Zeitschritt"). CLICK on the *Start!* button to run the simulation[4].

6. At the end of the simulation, the results are displayed in the *Outputs* tab of the GUI.

[1] Recall that the z_g-axis is defined positive in the direction of gravitational acceleration. An increase in altitude above the earth's surface will carry with it a decrease in the z_g-coordinate.

[2] This generates the *WinchSimulationParameters.mat* file which is used by the running simulation.

[3] Keep in mind that if the simulation reaches the previously defined cable release angle (automatic cable release) before the end of the *simulation duration*, the simulation will end automatically. If the simulation does not terminate through automatic cable release, the cable is then still attached and the glider is still somewhere between phases 3 and 5 of the winch launch.

[4] All other text boxes or input opportunities are already pre-loaded through other files or not connected to the winch simulation.

References

[Ale80] Alexander Schleicher GmbH, Alexander-Schleicher-Str. 1, D-36163 Poppenhausen (Wasserkuppe). *ASK 21 - Flug- und Wartungshandbuch*, April 1980.

[All80] W. Alles. *Untersuchungen zur manuellen, reglergestützten Führung eines Transportflugzeugs auf unkonventionellen Anflugbahnen.* PhD thesis, Technische Universität Braunschweig, 1980.

[All05] Wolfgang Alles. Flugmechanik i, ii. Skript zur Vorlesung 4, Lehrstuhl für Flugdynamik, RWTH Aachen, 2005.

[And07] John D. Anderson. *Fundamentals of Aerodynamics.* McGraw-Hill, 4 edition, 2007.

[Ape96] Karl-Heinz Apel. *Segelflug Praxis; Ausbildung, Weiterbildung, Inübunghaltung.* DAeC Wirtschaftsdienst GmbH, 2 edition, 1996.

[Bro01] Rudolf Brockhaus. *Flugregelung.* Springer-Verlag, 2 edition, 2001.

[DM04] P. Dietz and I. Mupende. Einfluss der seildämpfung auf die trommelbelastungen bei bewicklung mit kunststoffseilen oder kunststoff-stahl seilen. *Institutsmitteilungen - Institut für Maschinenwesen - TU Clausthal*, 29:5ff, 2004. Available from: `http://www.imw.tu-clausthal.de/fileadmin/Bilder/Forschung/Publikationen/Mitt_2004/01.pdf`.

[Etk98] Bernard Etkin. Stability of a towed body. *Journal of Aircraft*, 35(2):197ff, March-April 1998.

[Gäb07] Andreas Gäb. *Generische Simulation.* Lehrstuhl für Flugdynamik, RWTH Aachen, 2007. Available from: `http://www.dynamik.rwth-aachen.de/`.

[Gen08] General Motors Corporation, 300 Renaissance Center, P.O. Box 300, Detroit, MI 48265, USA. *GM Product Information on 2009 Duromax Diesel 6.6L V-8 Turbo (LMM)*, 2008. Available from: `http://media.gm.com/us/powertrain/en/product_services/2009/HPT%20Library/Diesel/2009_66L_LMM_SilveradoHDf.pdf`.

[Hen08] Rolf Henke. Flugzeusysteme. Skript zur Vorlesung 1, Institut für Luft- und Raumfahrt, RWTH Aachen, 2008.

[HK03] Klaus Henning and Sebastian Kutscha. *Informatik im Maschinenbau.* Aachener Reihe Mensch und Technik. Wissenschaftsverlag Mainz, 6 edition, 2003.

[HS98] Tobias Hofstetter and Gerhard Arnold Seiler. Projekt ak-7; nachrechung eines windenstart-energie-iterationsverfahrens. *47. Jahresbericht der Akademischen Fliegergruppe der Universität Karlsruhe e. V.*, 1998. Available from: `http://www.akaflieg.uni-karlsruhe.de/jahresberichte/jb98/jb98.pdf`.

[Joh93] G. Johannsen. *Mensch-Maschine-Systeme*. Springer Verlag, 1993.

[Klo07] Tobias Kloss. Simulation des windenstarts von segelflugzeugen. Studienarbeit, Lehrstuhl für Flugdynamik, RWTH Aachen, November 2007.

[KN00] Uwe Kiencke and Lars Nielsen. *Automotive Control Systems*. Springer Verlag, 2000.

[Mai93] Dieter Maier. *Segelfliegen; Theorie und Praxis*. nymphenburger in der F. A. Herbig Verlagsbuchhandlung GmbH, 3 edition, 1993.

[Pig96] Derek Piggott. *understanding Gliding; The Principles of Soaring Flight*. A & C Black (Publishers) Ltd, 3 edition, 1996.

[Rid98] J. C. Riddell. The effect of inertia in the winch launch. *Technical Soaring*, 22(3):91ff, 1998.

[Seg03] Segelflugkommision, Deutscher Aeroclub e. V. *Segelflugsport-Betriebs-Ordnung*, 2003. Available from: `http://www.daec.de/se/downfiles/sbo.pdf`.

[Sky08] Skylaunch Ltd, Unit E11-14, Wem Industrial Estate, Soulton Road, Wem, Shropshire, SY4 5SD, England. *Skylaunch 3 Daten und Fakten*, 2008. Available from: `http://www.skylaunch.de/windendaten.html`.

[Tec86] Technische Kommision, Deutscher Aeroclub e. V. *Betriebstüchtigkeitsanforderungen für Startwinden zum Starten von Segelflugzeugen und Motorseglern (BFST)*, 1986. Available from: `http://www.daec.de/te/downfiles/BFST.pdf`.

[Wil07] Wilhelm Nosbüsch GmbH, Schallbruch 59 D-42781 Haan / Rheinland. *TelWIS 2000, Der Fahrtmesser für den Windenfahrer*, 2007. Available from: `http://www.wilnos.de/TelWIS/TelWIS_Home.html`.

[WLO07] Paul Williams, Bas Lansdorp, and Wubbo Ockels. Modeling and control of a kite on a variable length flexible inelastic tether, August 2007. Available from: `http://www.lr.tudelft.nl/live/pagina.jsp?id=fe263f84-29af-4010-8222-2f1112c8f223&lang=en&binary=/doc/Kite%20modelling%20flexible%20tether_bas.pdf`.

[WV76] J. E. Williams and S. R. Vukelich. *The USAF Stability and Control Digital DATCOM, Volume I, Users Manual*. McDonnell Douglas Astronautics Company, St Louis, Missouri 63166, affdl-tr-76-45 edition, 1976. Available from: `http://www.holycows.net/datcom/USAF_DATCOM_UM.pdf`.